DISCLAIMER

This report was prepared as an account of work sponsored by an agency of the United States Government. Neither the United States Government nor any agency thereof, nor any of their employees, makes any warranty, express or implied, or assumes any legal liability or responsibility for the accuracy, completeness, or usefulness of any information, apparatus, product, or process disclosed, or represents that its use would not infringe privately owned rights. Reference herein to any specific commercial product, process, or service by trade name, trademark, manufacturer, or otherwise does not necessarily constitute or imply its endorsement, recommendation, or favoring by the United States Government or any agency thereof. The views and opinions of authors expressed herein do not necessarily state or reflect those of the United States Government or any agency thereof. Reference herein to any social initiative (including but not limited to Diversity, Equity, and Inclusion (DEI); Community Benefits Plans (CBP); Justice 40; etc.) is made by the Author independent of any current requirement by the United States Government and does not constitute or imply endorsement, recommendation, or support by the United States Government or any agency thereof.

ORNL/TM-2025/ 4072

Initial Design Curves for Alloy 709 for an Improved Creep-fatigue Design Method

Yanli Wang
Mark C. Messner

August 2025

Approved for public release.
Distribution is unlimited.

OAK RIDGE National Laboratory

ORNL IS MANAGED BY UT-BATTELLE LLC FOR THE US DEPARTMENT OF ENERGY

ORNL/TM-2025/ 4072

Materials Science and Technology Division

INITIAL DESIGN CURVES FOR ALLOY 709 FOR AN IMPROVED CREEP-FATIGUE DESIGN METHOD

Yanli Wang
Oak Ridge National Laboratory

Mark C. Messner
Argonne National Laboratory

Date Published: August 2025

Prepared by
OAK RIDGE NATIONAL LABORATORY
Oak Ridge, TN 37831
managed by
UT-BATTELLE LLC
for the
US DEPARTMENT OF ENERGY
under contract DE-AC05-00OR22725

Page intentionally left blank.

CONTENTS

LIST OF FIGURES

ABBREVIATIONS

ANL	Argonne National Laboratory
ART	Advanced Reactor Technologies
ASME	American Society of Mechanical Engineers
BPVC	Boiler and Pressure Vessel Code
CF	creep-fatigue
DOE	US Department of Energy
EPP	elastic-perfectly plastic
GCR	Gas-Cooled Reactors
INL	Idaho National Laboratory
NE	Office of Nuclear Energy
ORNL	Oak Ridge National Laboratory
p-SMT	internal-pressurized tubular simplified model test
SMT	simplified model test
US-NRC	U.S. Nuclear Regulatory Commission

ACKNOWLEDGMENTS

This research was sponsored by the US Department of Energy (DOE) under Contract No. DE-AC05-00OR22725 with Oak Ridge National Laboratory (ORNL), managed and operated by UT-Battelle LLC, and under Contract No. DEAC02- 06CH11357 with Argonne National Laboratory, managed and operated by UChicago Argonne LLC. Programmatic direction was provided by the Office of Nuclear Reactors of the Office of Nuclear Energy.

The authors wish to express their sincere gratitude to Kaatrin Abbott, DOE-NE Federal Manager, ART Fast Reactor Program (FRP); Matthew Hahn, Federal Program Manager, ART Gas-Cooled Reactors (GCR) Campaign; Bo Feng of Argonne National Laboratory, National Technical Director, ART FRP; and Gerhard Strydom of Idaho National Laboratory (INL), National Technical Director, ART GCR Campaign, for their invaluable support.

The following technical contributions are gratefully acknowledged: Xuesong Fan and ORNL student intern Yiming Chen for analyzing the data presented in this report; Bradley J. Hall and Charles Shane Hawkins of ORNL for conducting the fatigue and creep-fatigue experiments; and Heramb Mahajan of INL for providing fatigue and creep-fatigue data generated at INL.

Special thanks are extended to Ting-Leung Sham of US-NRC; and former NE-ART Materials Federal Program Manager Sue Lescia, and Subject Matter Expert Robert I. Jetter, for their tremendous support and insightful technical discussions in advancing the concept of an alternative creep-fatigue evaluation method over the years.

The time spent by Xuesong Fan and Zhili Feng of ORNL reviewing this report is acknowledged.

ABSTRACT

Creep-fatigue (CF) interaction damage is the primary damage mode for high-temperature structural components subjected to cyclic loading. Over the past several decades, researchers within the American Society of Mechanical Engineers (ASME) Boiler and Pressure Vessel Code (BPVC), Section III, Division 5, have focused on developing elevated temperature code rules to ensure conservative structural designs that mitigate CF failure in high-temperature reactors. The existing CF evaluation methodologies in the Code are based on the creep and fatigue damage diagram approach, which is complex and often excessively conservative. The alternative CF evaluation approach proposed here is intended to significantly simplify the evaluation procedure while reducing conservatism in high-temperature component design analysis.

This alternative CF evaluation method integrates the elastic–perfectly plastic (EPP) analysis approach with the simplified model test (SMT) CF design concept, leveraging the advantages of both methods. This report presents the preliminary analysis and the approach for developing CF design curves for Alloy 709, utilizing fatigue and CF data generated for the 100,000-hr Code Case to support its qualification to ASME Section III, Division 5 for Class A construction of high temperature reactors. This study is to support the incorporation of Alloy 709 in this alternative CF evaluation method. Recommendations for the remaining work needed to complete the effort are also provided.

1. INTRODUCTION

Materials subjected to cyclic deformation at elevated temperatures experience both creep and fatigue damage. These two mechanisms can interact, significantly impacting on the overall performance and long-term integrity of the material. Creep-fatigue (CF) interaction damage under cyclic loading at elevated temperatures is often more detrimental than either pure fatigue or pure creep damage alone. Advancements in CF evaluation of high temperature components are crucial for improving the economic viability of high-temperature reactors.

The current evaluation procedure for CF damage in Subsection HB, Subpart B of BPVC Section III, Division 5 relies on the bilinear creep and fatigue damage diagram, known as the D-diagram approach. However, D-diagram based CF evaluation methods are complex and often lead to excessively conservative designs, which arises from how the damage envelop was constructed from the standard CF data, along with the conservative procedures used in the CF design analysis.

The development of an alternative CF evaluation methodology has been an important effort under DOE's High-Temperature Design Method development program. This integrated approach—combining the elastic–perfectly plastic (EPP) analysis method with the simplified model test (SMT) design methodology, referred to as the EPP-SMT method—has been identified as a viable alternative for evaluating CF in the design of pressure boundary components for high-temperature reactors (Wang, 2024). A key advantage of this new approach is that it eliminates the need for a damage interaction diagram, significantly simplifying the design procedure without introducing excessive conservatism. The ASME Section III Division 5 Code Committee has acknowledged the advantages of this alternative CF evaluation methodology and identified it as a priority item for committee actions.

The development of EPP-SMT CF design curves relies on the availability of experimental data and a well-calibrated inelastic model capable of reasonably accurate life-cycle predictions under long hold-time conditions. Leveraging the extensive CF testing data generated under the DOE's effort to qualify Alloy 709 for the ASME Code, this report presents a preliminary analysis and develops draft CF curves for Alloy 709 at various temperatures. Additional data needs and design analyses required to finalize the CF design curves are outlined as part of the proposed future work

2. ALTERNATIVE CREEP-FATIGUE EVALUATION METHOD

2.1 CONCEPT OF THE ALTERNATIVE CREEP-FATIGUE EVALUATION METHOD

The integrated EPP-SMT design method leverages the strengths of both approaches to provide an alternative CF evaluation methodology that is simpler to implement, avoids excessive conservatism, and offers reasonable assurance in the safe design of high-temperature pressure boundary components subjected to cyclic loading in the creep regime, as illustrated in Figure 1 (Wang, 2024). The key characteristics are the following:

- The newly developed EPP analysis methodologies significantly simplify the design process by eliminating the need for stress classification and accounting for stress and strain redistribution through the concept of a pseudo yield strength, defined with consideration of high-temperature creep effects. The EPP method (Code Case N-861, 2021) is far simpler to apply than a full inelastic analysis.

- The SMT experiments are designed to replicate or bound the key features of actual components operating in the creep regime, effectively accounting for stress and strain redistribution and the increased creep damage that develops around localized defects and stress risers (Wang, 2024). The SMT experimental data-based CF design curves are developed in terms of the strain range versus cycles to failure (Figure 2) with design margins.

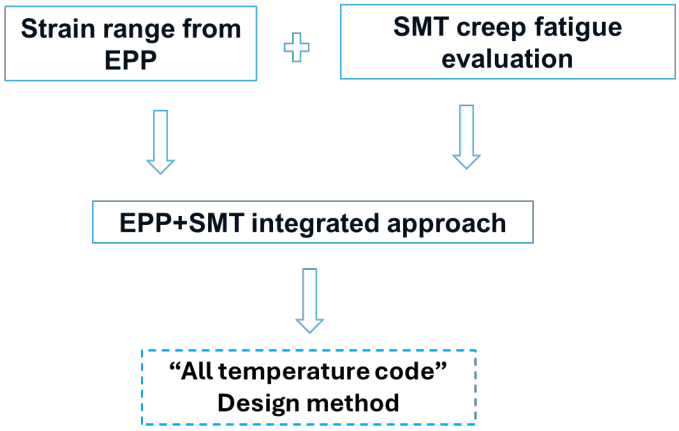

Figure 1. Concept of the EPP-SMT approach

In developing the EPP-SMT method, the correlating parameters are the calculated maximum strain in the structural component design problem and the strain range in the SMT test article. The maximum strain ranges for both the high temperature component and the SMT test specimens are determined using the EPP strain limits procedure outlined in Code Case N-861. The CF design curves include the effects of hold time duration and the necessary adjustments to account for stress and strain redistribution due to creep effect without being excessively conservative.

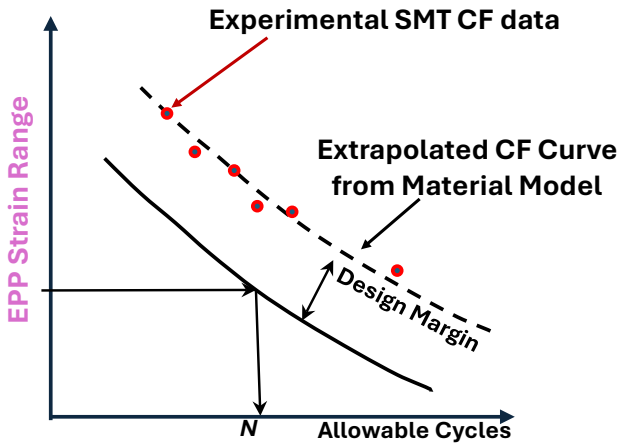

Figure 2. Conceptual overview of the EPP-SMT methodology.

The evaluation procedure using this EPP-SMT approach is essentially the same as that used in ASME Section III Division 1 Subsection NB, where the damage fraction is determined as the ratio of number of cycles in the design problem to the allowed number of cycles in the CF design curves.

In practice, generating the experimental SMT CF data required to establish the design curve is often impractical due to long experiment duration, particularly at low strain ranges and extended hold times. In this study, a well-calibrated material constitutive model developed at ANL was used to generate the information needed for developing the EPP-SMT CF design curves.

2.2 KEY FACTORS FOR CONSIDERATION

2.2.1 Elastic follow-up effect and local stresses

In high-temperature structural components under cyclic loading, creep deformation can lead to stress and strain redistribution at stress riser locations, including both structural and metallurgical discontinuities locally, or due to globally structural constraint effect. This phenomenon is known as the "elastic follow-up" effect. As discussed in more details in our previous studies (Wang, et al, 2014, 2016a, 2016b, 2017a, 2017b, 2018, 2019, 2020, 2021a, 2021b, 2024), elastic follow-up can cause much larger accumulated strains in structures subjected to displacement-controlled loading than those predicted by elastic analysis. This effect accelerates damage to the material and may cause premature failure in components under long-term loading.

SMT experiments utilize a two-bar geometry to bound the response of a high-temperature component. While there is no rigorous method to conclusively demonstrate that this two-bar model can bound the deformation of a structural component under all conditions, approaches based on a four-bar model representation of the stepped cylinder can be employed to show that the bounding strategy is applicable across a variety of practical scenarios (Kasahara et al. 1995; Jetter 1998).

Referring to Figure 3, elastic follow-up can be quantified by calculating the ratio of the creep strain in the test section of a component—including the effects of elastic follow-up, ε_{0-2}, —to the creep strain that would have occurred under pure relaxation, ε_{0-1}. The latter represents the condition where standard strain-controlled CF is conducted on a laboratory-scale test coupon specimen.

Thus, the elastic follow-up factor, q, is given by:

$$q = (\varepsilon_{0-2})/(\varepsilon_{0-1}) \quad (1)$$

Messner et al. (2019) described a method for determining the elastic follow-up factor in 3D finite element calculations as a function of position and time from finite element simulations. They demonstrated that classical elastic-creep solutions can be utilized to assess elastic follow-up and to develop representative values for high-temperature components.

As discussed by Jetter (1998) and Takahura et al. (1995), the value of global follow-up is conservatively represented by $q_n = 2$, and is certainly bounded by a value of 3, and a peak elastic follow-up for an SMT specimen should be in the range of 4.0 to 4.5 to adequately bound the response of the structures of interest.

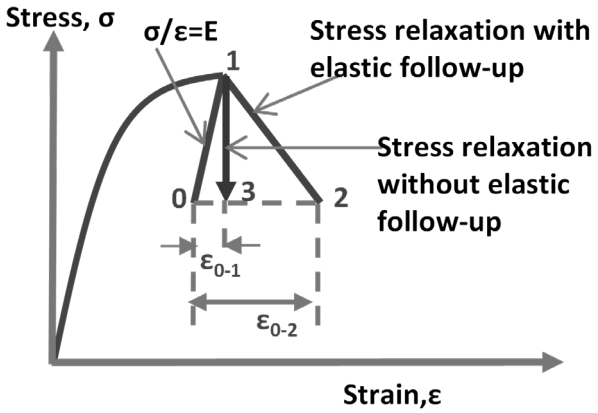

Figure 3. Elastic follow-up.

Another key factor is high stress concentration in areas with structural or metallurgical discontinuities. Significant global elastic follow-up can lead to a nonlinear increase in localized strain range, resulting in accelerated creep damage, and premature failure.

2.2.2 Effect of primary sustained load

To evaluate the effect of primary sustained load, Wang et al. (2020, 2021a, 2021b) extended the SMT method to internal pressurized tubular specimens, i.e., p-SMT, at 950°C on Alloy 617. The sustained primary load was introduced by internal pressure to a tubular SMT sample. The test results from this study along with the original p-SMT data on Alloy 617, demonstrated that although internal pressure is within the allowable stress limit per ASME Section III, Division 5, the SMT CF cycles to failure were reduced for the cases tested with primary-pressure load. The reduction of SMT CF life because of primary load was found to be dependent on strain ranges, temperatures and elastic follow-up factors.

Approaches to account for the primary-load effect on SMT design curves were discussed in Barua et al. (2020, 2021), and the analysis results show that the EPP strain range analysis procedure naturally captures the primary pressure effect. Barua et al. (2020, 2021) also demonstrated that the EPP-SMT methodology is much simpler to execute than the conventional CF damage analyses through multiple sample problems. The remaining critical factors in finalizing the SMT-based design curves are the methods for extrapolating

the design curves to the low strain range region and with longer hold times (such as long hold time of 1,000-hr or longer) that are prototypical of plant operations.

3. EPP-SMT CREEP-FATIGUE EVALUATION FOR ALLOY 709

3.1 DISSIPATED WORK BASED METHOD FOR CREEP-FATIGUE LIFE PREDICTION

In our recent studies (Hou et al. 2023a and 2023b; Wang et al. 2023), it was concluded that the time fraction-based method was overly conservative for predicting the CF life cycles for Alloy 617, while the dissipated work-based method provided a more accurate prediction of CF performance at elevated temperatures. In this study, dissipated work approach is evaluated for developing the EPP-SMT design fatigue curves for Alloy 709.

The available Alloy 709 CF test data are, by necessity, for higher strain ranges and shorter hold times than actual high temperature reactor components. Here we correlate the failure data from the tests to the amount of work the material dissipates up to the point of failure. This dissipated work can be calculated as the area inside the stress-strain hysteresis loops in the experiments or in simulations of creep-fatigue type tests:

$$W = \int \sigma d\varepsilon$$

with σ the uniaxial stress and ε the (mechanical) strain. The dissipated work was calculated from the hysteresis loops, represented by the shaded area in Figure 4.

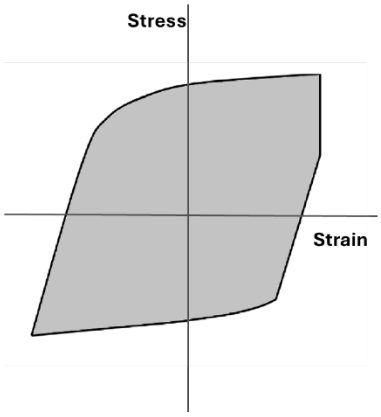

Figure 4. Dissipated work in a hysteresis loop.

Hou et al. (2023a) demonstrated that the accumulated dissipated work is approximately linearly proportional to the number of applied cycles once the CF process reaches a steady state by analyzing available data alongside the corresponding hysteresis loops. This finding offers advantages in developing EPP-SMT CF design curve, as it allows for the use of a limited number of CF test cycles to extrapolate results for CF failure cycles effectively.

3.2 FAILURE CRITERIA BASED ON ACCUMULATED DISSIPATED WORK OF CF EXPERIMENTS

The amount of accumulated dissipated work at failure depends on the testing conditions. The experimental data with complete hysteresis loops have been generated from standard CF testing, as part of the Code Case

data package generated at ORNL and INL in support of the ASME Code qualification for Alloy 709. Partial data package consisting of the CF and pure fatigue testing results available for this study at the time of writing this report were analyzed, and the results are summarized here.

Pure fatigue: the dissipated work at mid-life cycles and the total accumulated work at failure were collected for pure fatigue testing data of the three heats of Alloy 709 for room temperature, 427 °C, 760 °C and 816°C, in Figure 5. The mid-life cycle represents the stabilized hysteresis loop.

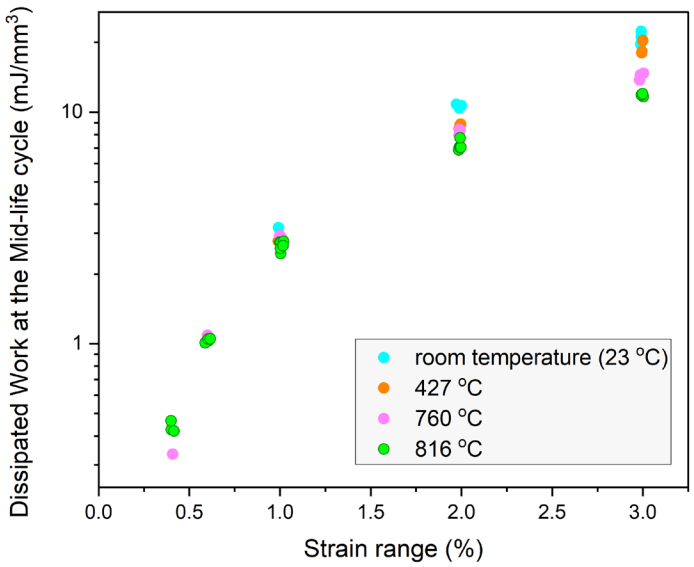

(a)

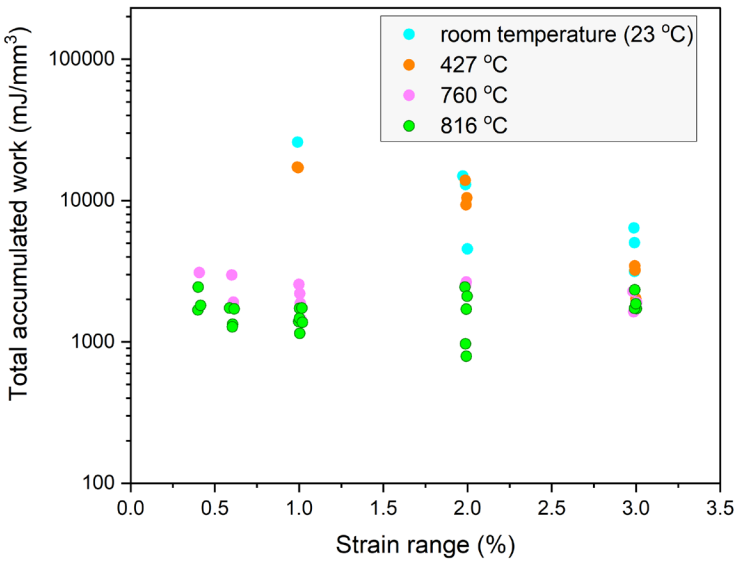

(b)

Figure 5. Pure fatigue tests on Alloy 709: (a) Dissipated work at mid-life cycle and (b) Total accumulated dissipated work at failure.

As demonstrated in analyzing these pure fatigue test data,

- The dissipated work at mid-life cycle increases with strain range at each test temperature. When the strain range exceeds a certain threshold (e.g., 0.6%), it begins to decrease with increasing temperature. At 816°C, it shows the lowest values of these four temperatures evaluated.
- However, the total accumulated dissipated work approached saturated value for the two higher test temperatures of 760 °C and 816°C.

Creep-fatigue: Standard CF test data collected at 816°C from three heats of Alloy 709, all conducted with an elastic follow-up factor of 1, were analyzed. The dissipated work at mid-life cycles and the total accumulated work at failure are presented in Figure 6 and Figure 7. These CF tests covered strain ranges from 0.4% to 3% and included tensile hold times of up to 3600 seconds. Additionally, one test with an elastic follow-up factor of 3 and an average strain range of 0.33% was included in the plots. The results show that:

- The dissipated work at mid-life cycle increases with strain range; however, the tensile hold time has minimal effect, indicating a saturation effect at 816°C.

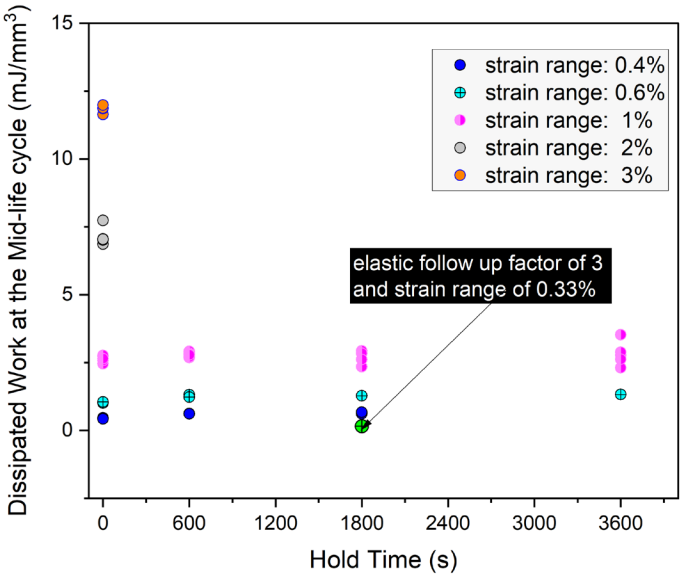

Figure 6. Creep- fatigue tests on Alloy 709 at 816°C with dissipated work at mid-life cycle

- The total accumulated dissipated work shows the most significant reduction with the introduction of the initial tensile hold-time but appears to approach saturation when the hold time reaches 1800 seconds or longer. Although there is considerable data scatter, lower strain ranges tend to result in lower accumulated dissipated work at this test temperature, though all values remain within the same order of magnitude at this temperature. The use of an elastic follow-up factor of 3 did not significantly reduce the total accumulated work.

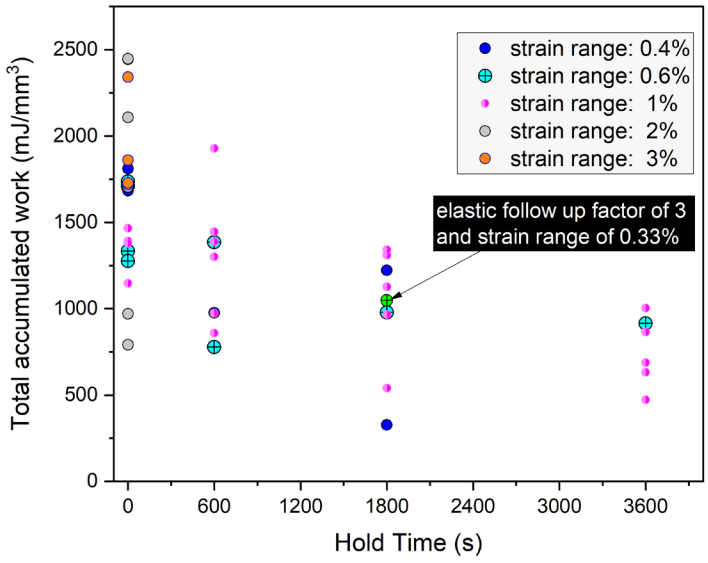

Figure 7. Creep- fatigue tests on Alloy 709 at 816°C with total accumulated dissipated work at failure.

3.3 EXTRAPOLATION METHOD

Due to the impractically long test durations required to generate failure data at low strain ranges and extended hold times, a well-calibrated constitutive material model must be developed to accurately describe the material's CF deformation behavior at various temperatures for design curve extrapolation. To this end, the accumulated dissipated work extrapolated from the newly calibrated material model was compared to the experimental data at temperature range of interest between 850 °C to 954 °C, with the results presented in the following sections.

3.3.1 Inelastic Model validation

To extend the available test data to component strain ranges and hold times we use an inelastic constitutive model to predict the dissipated work for the unavailable test conditions. The model we used is described in (Bhesania and Messner, 2025). The model has a Kocks-Mecking type flow rule to capture both creep and cyclic inelastic deformation and a simple combined isotropic and kinematic hardening model to describe the evolution of monotonic and cyclic hardening in the material. The model was trained against the entire Alloy 709 test data set including the cyclic tests but also creep, tension, and strain rate jump data. The full model is stochastic, defined by statistical distributions of the model parameters. The model can be sampled by repeatedly simulating an experimental condition and recording the predicted values, finally examining the statistical distribution of the predictions against the distribution of the test data.

The report (Bhesania and Messner, 2025) describing the model in detail provides a complete mathematical description of the model, the trained model parameters, and a more complete description of how the model was validated against test data. However, given the importance of accurately capturing the dissipation of Alloy 709 under cyclic conditions this section examines how accurately the model represents this dissipation.

There are 70 cyclic tests, including both strain-controlled fatigue and creep-fatigue, in the Alloy 709 training database used to calibrate the model. Figure 8 is a one-to-one plot showing the predicted dissipation in the steady state condition over a single cycle from the model versus the measured dissipation in the actual test. The figure shows error bars representing a 90% prediction interval from the statistical model in addition to the median result. Figure 8(a) and Figure 8(b) plot the same data, (a) shows the predictions on a linear scale and (b) on a log scale to better visualize the results at the smaller values.

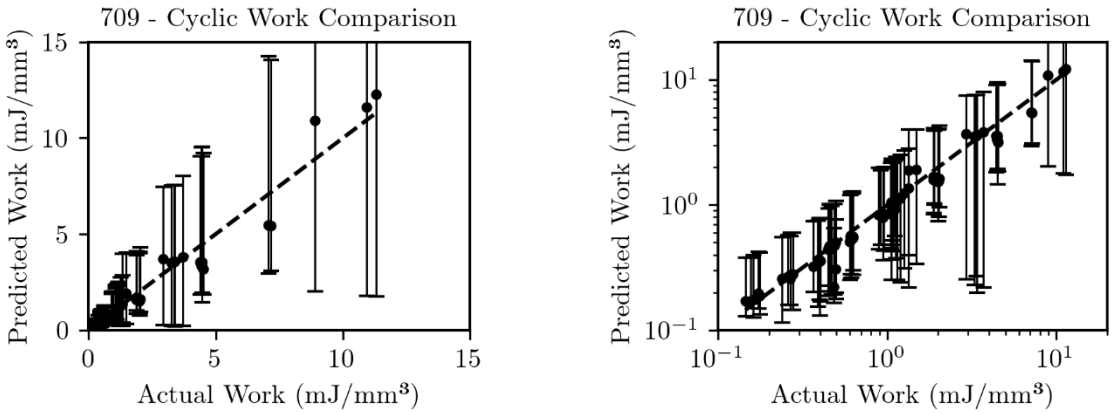

(a) (b)

Figure 8. Actual vs. predicted energy dissipation per cycle in steady-state conditions: (a) Linear Scale, (b) Log Scale

The plots demonstrate the 709 inelastic model accurately captures the amount of dissipation per cycle in the steady state. The average predicted response closely follows the one-to-one line and all the test data fall in the 90% prediction intervals.

Appendix A provides additional validation by plotting the dissipation as a function of test cycle count for all the available experiments along with the actual and predicted stress-strain hysteresis loops. These provide more detailed validation against the cyclic data, but also justify using the 50th cycle to represent the stable dissipation per cycle in the next section. By this cycle count all the experimental data and model predictions have stabilized. Specifically, the stress-strain hysteresis loops are not changing significantly cycle-to-cycle and the amount of work dissipated per cycle has become constant (so the accumulated dissipation per cycle is linear).

3.3.2 Predicted dissipation work

As discussed in Section 3.2, the general trends in the predicted dissipation are what we would expect from a basic understanding of material inelasticity, with one exception. Dissipated work per cycle increases when:

- The temperature increases, to a point.
- The strain range increases.
- The hold time increases.

Figure 9 illustrates each trend. The main difference between typical material behavior and the model predictions is the temperature dependence. Dissipation per cycle increases as the temperature increases up to around 750 °C, but then decreases beyond that point. Similarly, at higher temperatures the amount of dissipation per cycle becomes insensitive to the hold time.

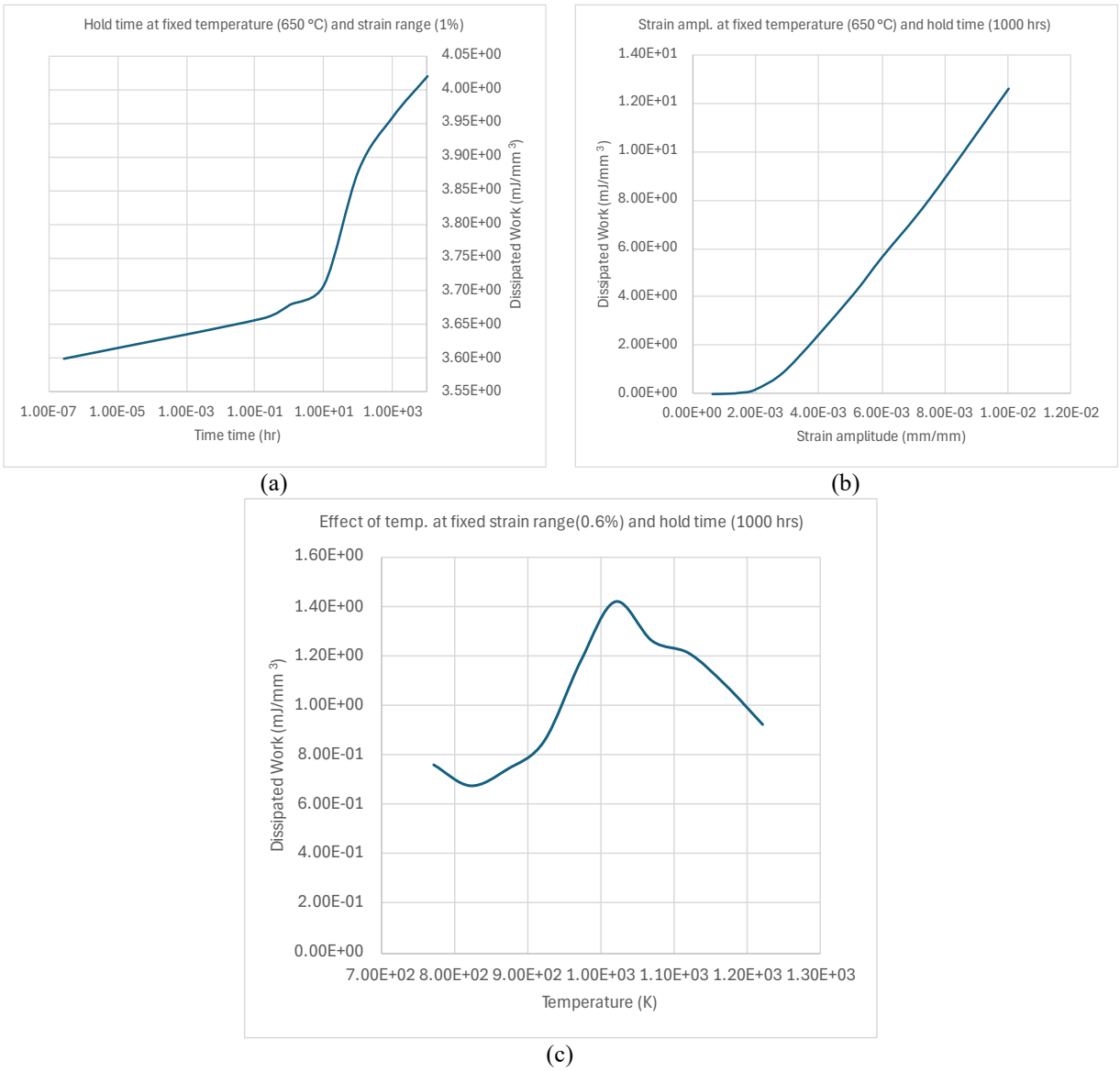

Figure 9. General trends in dissipation as a function of hold time (a), strain range (b), and temperature (c).

The reduction in dissipation per cycle at similar conditions for temperatures above 750 °C is also evident from the experimental data. Figure 10 plots the dissipation per cycle for all CF tests. The red points and trend line are the tests at similar conditions (short hold times, strain ranges of 0.6%). Both in general and at specific conditions, the material dissipates less work per cycle as temperature increases at the hottest conditions.

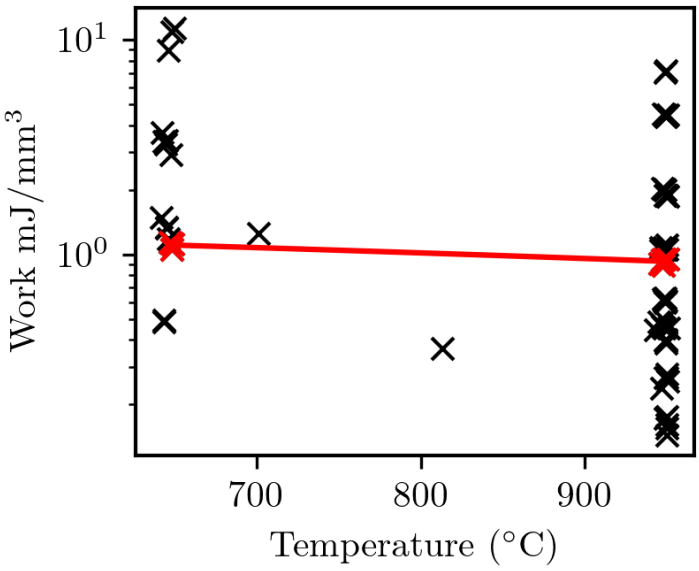

Figure 10. Dissipation per cycle for the creep-fatigue data plotted versus temperature. Red points are at similar test conditions.

3.4 VERIFYING THE EPP STRAIN RANGE APPROXIMATION

The EPP+SMT approach requires calculating the mechanical strain range experienced by a component at each location over a given load cycle. Previous work (Barua, et al, 2021, Messner et al 2018, and Barua and Messner 2024) on the EPP+SMT method recommended an EPP calculation with a pseudoyield stress defined as the lesser of:

- The ASME design yield strength S_y at a given temperature
- The 0.2% offset yield strength from the isochronous stress/strain curve for the material at a given temperature and the load cycle period.

Past results indicate this EPP calculated strain range conservatively bounds both measured and more accurately simulated (i.e. with a cyclic viscoplastic material model) strain ranges. This section verifies this result for Alloy 709.

The values of the isochronous stress-strain curves used in these calculations are those that will be proposed for incorporating the material into Section III, Division 5 of the ASME Code via a Nuclear Code Case. The ISSC models along with detailed validation will be reported in a forthcoming ANL technical report. An earlier report (Barua and Messner 2024) provides initial versions of the curves, but the final proposed models vary from this preliminary description.

3.4.1 p-SMT geometry

The first verification comparison uses the p-SMT test geometry itself as a representative quasi-component (Wang et al., 2019). This test article geometry, discussed elsewhere in the report, combines biaxial primary load via internal pressure with secondary load via displacement-controlled axial displacement,

delivered through elastic follow up and including a hold at fixed displacement. The test article therefore includes all the key structural factors thought to affect creep-fatigue failure in the ASME Boiler Code.

This verification example simulated the p-SMT geometry under different combinations of pressure, temperature, axial displacement, and hold time. The examples fix the temperature to 700 °C and the pressure to 10 MPa (roughly 1/3 of the value of the allowable stress S_o at this temperature) and vary the axial displacement and the hold time, considering combinations of displacement amplitudes of 0.025, 0.05, 0.1, and 0.15 mm and hold times of 1, 100, and 10,000 hours. These parameters span strain ranges and cycle periods ranging from accelerated test conditions, like the actual p-SMT tests, down to small strain ranges with long hold times more indicative of operating components.

This example compares the strain ranges calculated by the EPP method in steady conditions to the strain range calculated by inelastic analysis using the detailed constitutive model for Alloy 709 described in a previous chapter and used to extrapolate the amount of work dissipated per cycle. The goal for the EPP method is to be more conservative, i.e. large, compared to the more accurate calculation with the inelastic model.

Figure 11 plots a one-to-one diagram comparing the EPP and inelastic strain ranges calculated for each case. In all cases except one the EPP strain range is greater than or equal to the inelastic strain range.

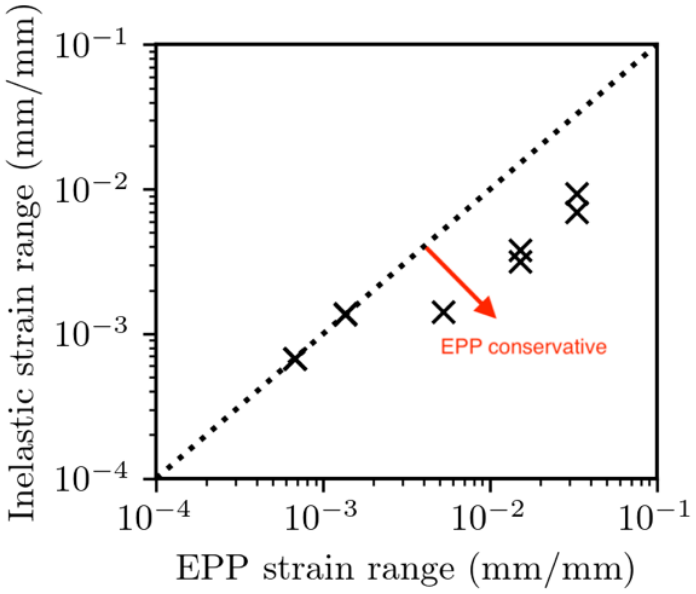

Figure 11. Comparison of EPP and inelastic strain ranges: dotted line indicates one-to-one line; arrow shows conservative side for EPP

At smaller values of the strain range the specimen response remains nearly entirely elastic. Under these conditions the inelastic and EPP strain ranges exactly agree, as both have the same elastic constants. At larger values of the strain range, corresponding to longer hold times and/or larger displacements, the EPP strain ranges conservatively bound the inelastic calculations.

In one case the EPP strain range is slightly smaller than the inelastic strain range. This difference is imperceptible on the diagram. In this condition the inelastic model predicts a very small amount of additional strain due to creep whereas the EPP model is elastic in the steady state. The reason for this

single non-conservative result is using the 0.2% offset of the isochronous curve, rather than a proportional limit, for the psueodyield stress definition. This definition allows for a small amount of creep strain, by definition less than 0.2%, in the EPP calculation before it affects the EPP results. These differences are small compared to the more accurate calculation and switching to a proportional limit definition for the ISSC would further increase the conservativeness of the method for larger true strain ranges. Hence, we retain our recommendation to use the EPP method based on the cycle period 0.2% offset stress.

3.4.2 Component simulation

Figure 12 describes a representative component simulation. The component is an axisymmetric flat head vessel supported by the edge of the head. The vessel is under internal pressure plus a static load on the top of the head. The left side of the axisymmetric component drawing defines the geometry; the right side defines the loading and support conditions. The vessel temperatures vary periodically, driven by the temperature histories of the blue and red regions labeled on the plot. The vessel is perfectly insulated on all surfaces except the blue and red regions. The red region remains at a fixed temperature while the blue region varies from the initial, hot temperature, to a lower temperature, and back, including a hold at the cold end of the cycle.

The specific problem geometry is defined by $d = 3000$, $l = 2000$, $t_s = 50$, $t = 150$, and $s = 250$ mm. The load cycle is defined by an internal pressure of $p = 0.5$ MPa, a top load of $q = 2.0$ MPa, an initial hot temperature of $T_0 = 700$ °C, and a cold temperature of $T_c = 200$ °C. The mechanical loads are ramped over $t_r = 1$ hr and the temperature cycle is defined by $t_t = 5$ and $t_h = 30$ hr.

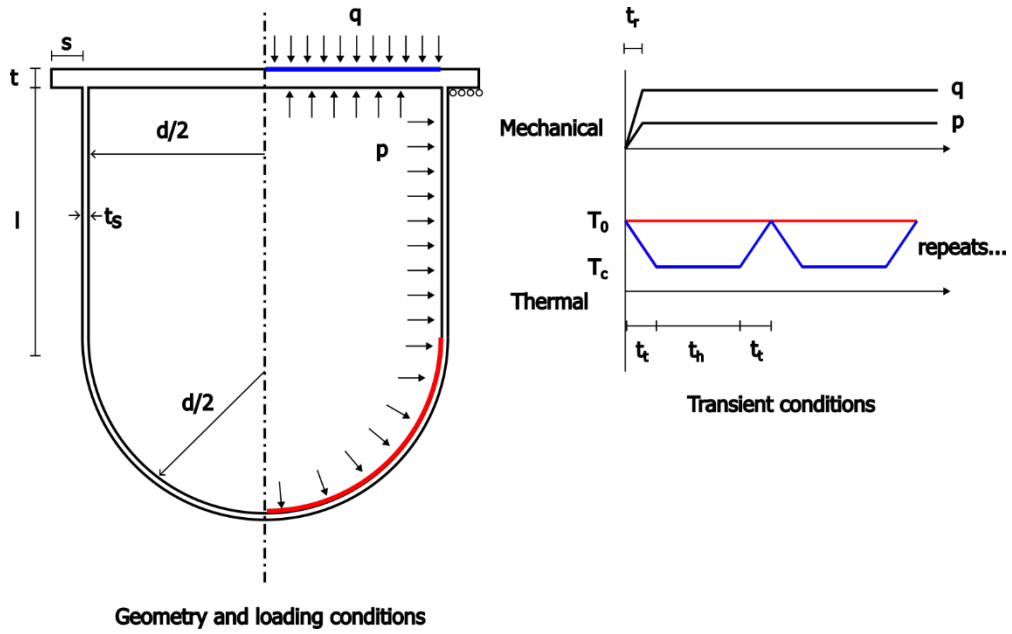

Figure 12. Flat head vessel sample component problem.

The vessel is constructed from Alloy 709. We ran two simulations, one with the full inelastic constitutive model used in the dissipated work calculations and a second with an EPP material model, using the pseudoyield stress for the EPP+SMT method defined above. The design yield stress S_y controls the values of the pseudoyield stress, except at the 700 °C and above. Both models apply the same elastic and thermal properties, found in Section II, Part D for the material.

Figure 13 shows representative diagrams of the vessel temperature and the von Mises stress both in the middle of one of the temperature excursions (the stresses in this figure come from the inelastic constitutive model). The figure demonstrates the thermal gradient that builds between the cold head and the warm vessel. This temperature difference leads to differential expansion between the head and the shell, with the head contracting more, leading to large stresses at the head/shell connection. The figures both plot the vessel shape with exaggerated (10x) displacements to demonstrate the distortion caused by the differential thermal contraction.

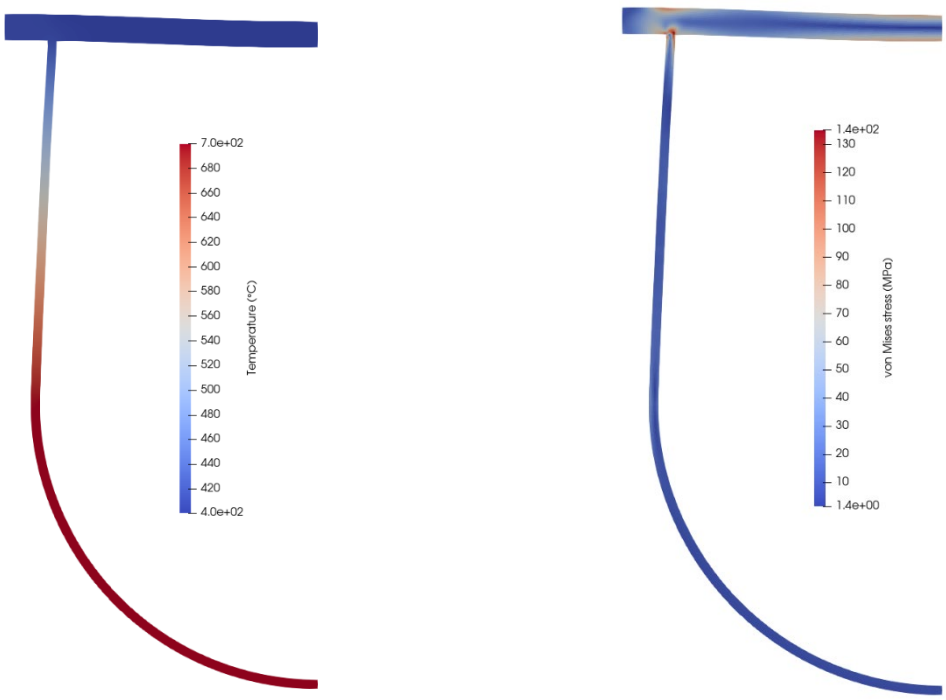

Figure 13. (a) temperature and (b) von Mises stress during one of the low temperature excursions.

Figure 14 plots the maximum strain range over a single repeated cycle of the periodic thermal load, specifically the 20th repetition. Figure 14(a) shows the results for the inelastic calculation and Figure 14(b) for the EPP calculation. Unsurprisingly, the maximum strain range in both models is located near the shell/head connection. This figure plots the range of values for the EPP and inelastic calculations in the same color scheme and demonstrates the inelastic strain range is smaller everywhere in the model than the EPP strain range. Therefore, applying the EPP approach to calculating the strain ranges provides a conservative estimate for the SMT creep-fatigue life evaluation.

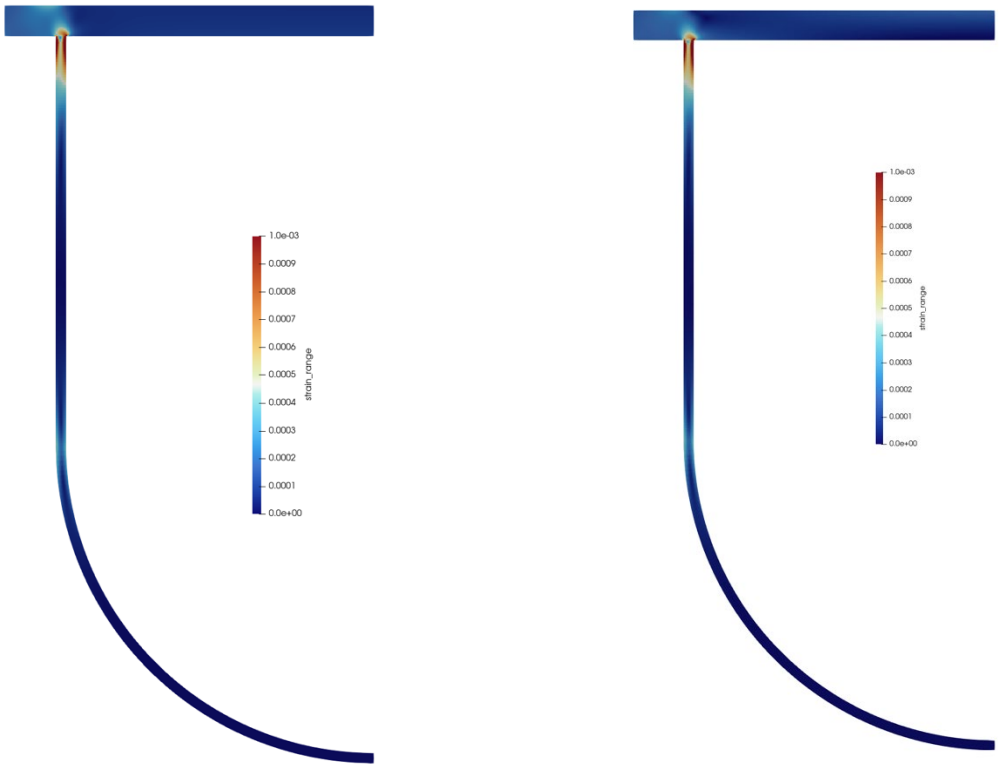

(a) (b)

Figure 14. Comparison between the strain range calculated by inelastic analysis (a) and the EPP analysis (b) for the vessel problem at the time during the final cycle giving the largest strain range in both simulations.

4. PRELIMINARY EPP-SMT CREEP-FATIGUE CURVES FOR ALLOY 709

In this study, the cycles to failure were extrapolated using the dissipated work from a limited number of cycles output by the material model at ANL, once the hysteresis loop reached steady state. The cut-off value of 327 mJ/mm^3, the lowest value was used as the critical value for CF failure data up to 816 ºC, was used as the failure criteria. The analysis considered strain ranges of 0.02, 0.015, 0.012, 0.01, 0.006, 0.004, 0.003, 0.0025, 0.0015, and 0.0013, and hold times of 600-seconds, 1-hr, 10-hr, 100-hr, and 1000-hr at each strain range.

The extrapolated CF failure cycles as a function of strain range and hold times are shown in Figure 15, Figure 16 and Figure 17 for temperatures of 450°C, 600°C, 650°C, 700°C, 800°C and 850 °C, respectively. These curves represent the "best-estimate" predictions for cycles to CF failure. Each figure includes the predicted pure fatigue curve, as well as CF curves with tensile hold times of 1 hour and 10,000 hours.

For reference, the predicted lower-bound pure fatigue curves—based on the 90% prediction interval of the dissipated work per cycle—are also included for temperatures between 450 °C and 700 °C. Interestingly, these lower-bound fatigue curves conservatively envelop the predicted CF curves, even at the 10,000-hour tensile hold time.

Experimental data at 650 °C are included to demonstrate the conservative nature of the CF design curve predictions. This result aligns with expectations, as the analysis in Section 3 shows that the critical value for CF failure generally increases at lower temperatures. The critical value of 327 mJ/mm³ used in generating the preliminary curves was derived from a test conducted at 816 °C, making it a conservative estimate for predictions at lower temperatures.

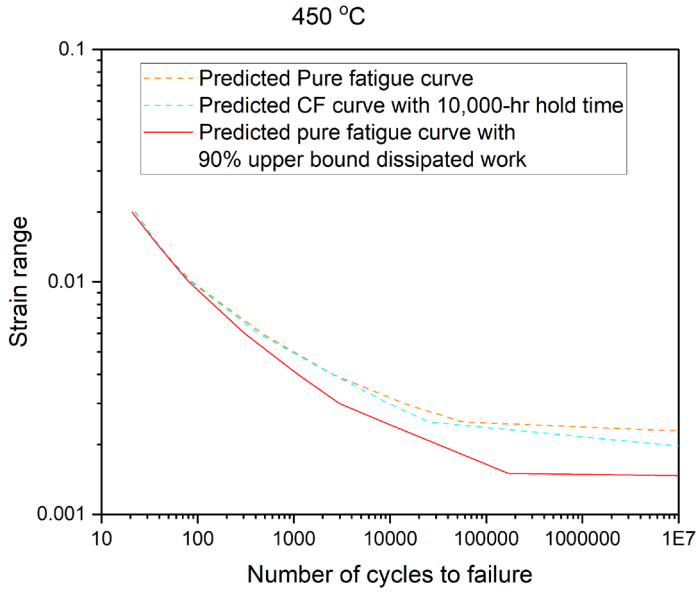

(a)

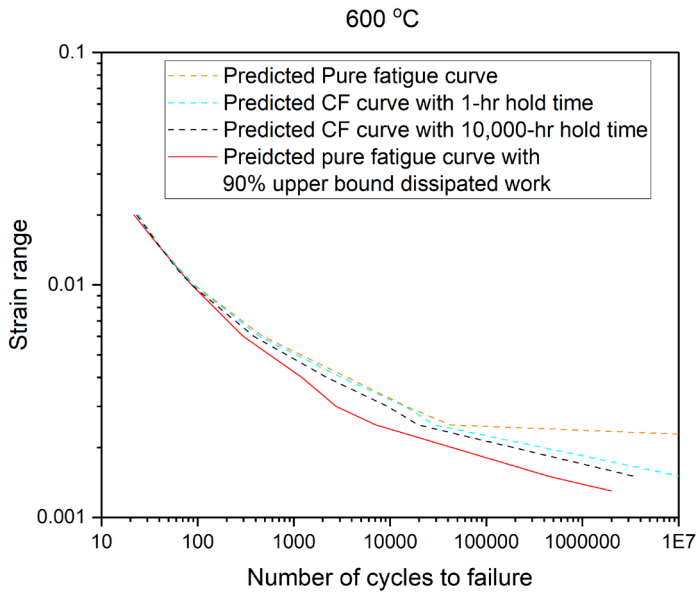

(b)

Figure 15. Alloy 709 creep-fatigue curves at (a) 450 °C and 600 °C

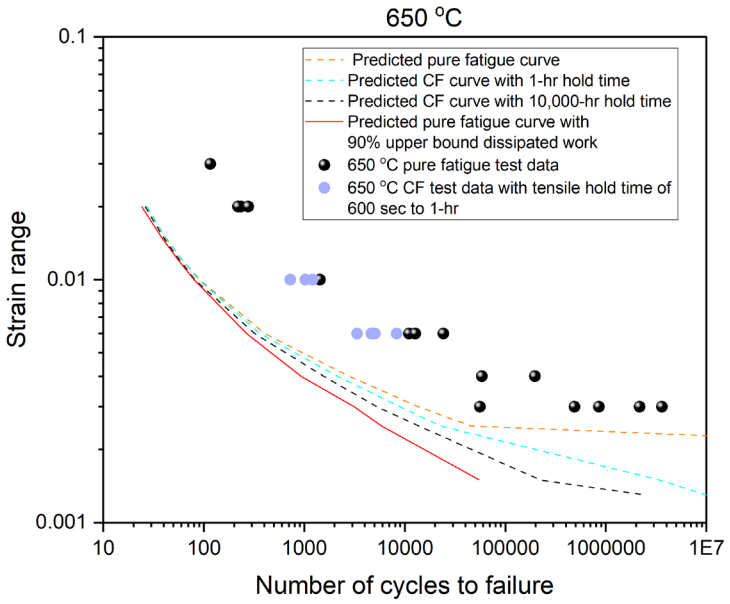

(a)

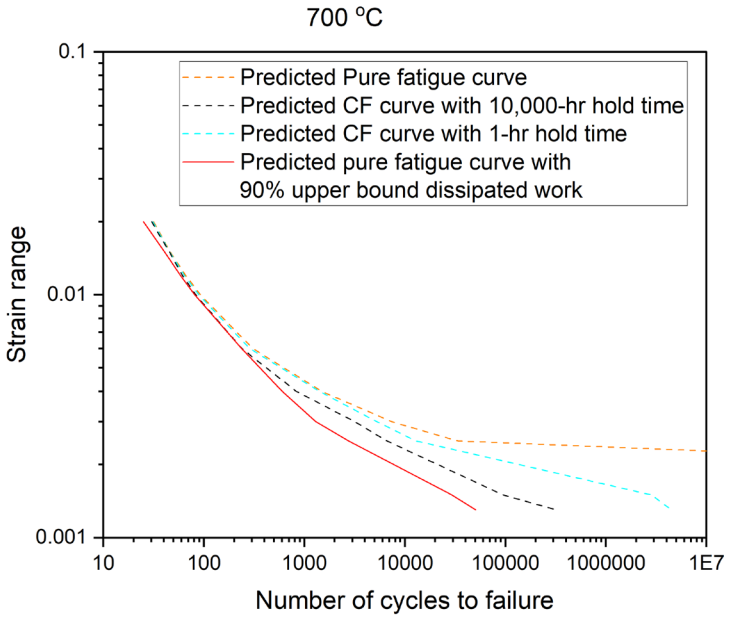

(b)

Figure 16. Alloy 709 creep-fatigue curves at (a) 650 °C and 700 °C

Experimental data at 816 °C are plotted alongside the predicted fatigue and CF curves for 850 °C, showing that the predicted curves at this slightly higher temperature successfully envelope all experimental results at lower testing temperature. Compared to the predictions at 650 °C, the best-estimate curves at 850 °C exhibit reduced conservatism.

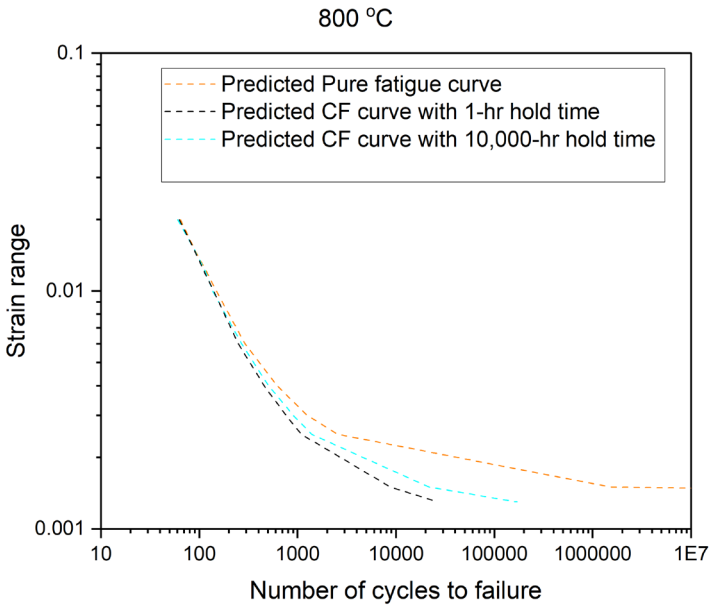

(a)

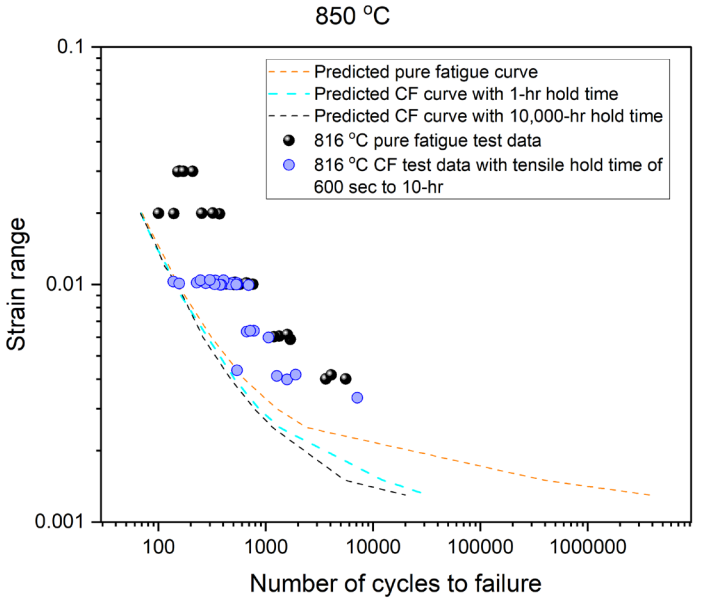

(a)

Figure 17. Alloy 709 creep-fatigue curves at (a) 800 °C and 850 °C

5. SUMMARY AND RECOMMENDED FUTURE WORK

This report summarizes the preliminary analysis of an alternative creep-fatigue (CF) evaluation method based on the EPP-SMT approach for Alloy 709. To support the extrapolation of EPP-SMT CF design curves for long hold times, a newly calibrated material constitutive model developed by ANL was utilized to provide the required input. The data package prepared for the Alloy 709 100,000-hr code case proved sufficient for calibrating an accurate material model, developed at ANL, suitable for generating the alternative CF design curves. The extrapolated best-estimated CF curves consistently envelop both SMT CF experimental data and standard CF test results for Alloy 709 across a broad temperature range. The report also presents sample problems and demonstrates that the EPP strain range conservatively bounds the maximum strain ranges observed in components.

Recommendations for future work include the following:

- It is recommended that a set of CF design curves be developed for Alloy 709 at 954 °C. The data package prepared in support of the Alloy 709 100,000-hr Code Case contains sufficient information to support design at this temperature for shorter-term excursions. Additionally, fatigue design curves at 954 °C are already available as part of the data package. Having a full set of CF design curves at 954 °C is beneficial for providing flexibility in creep-fatigue design analysis.

- It is also recommended that the EPP-SMT CF design curves for Alloy 709 be constructed using reduction factors applied to both cycles to failure and strain ranges, following the conventional approach. Specifically, the design curves are determined as the lower of two curves, obtained by applying a reduction factor of two on the strain range and a reduction factor of twenty on the cycles to failure, to provide reasonable conservative design CF curves.

- Previous work on Alloy 617 by Wang et al. (2017a, 2017b) demonstrated that primary pressure loading can reduce CF life. Therefore, further evaluation of the effect of primary pressure on Alloy 709 at various temperatures is warranted, both experimentally and analytically. Additional SMT experimental results also are beneficial in verification of the EPP-SMT CF design curves.

- There are existing CF evaluation methodologies in the ASME Section III Division 5, High Temperature Reactors Code that are based on creep and fatigue damage diagram, and these approaches will be included as part of the Alloy 709 100,000-hr Code Case. Comparing these existing methods with the alternative CF design curves presented in this report is useful for assessing the effectiveness of the alternative approach—both in terms of ease of implementation and the potential for reducing unnecessary conservatism.

REFERENCE

ASME Boiler and Pressure Vessel Code, (2025), “Rules for construction of Nuclear Facility Components”, Division 1-subsection NB Class 1 Components, American Society of Mechanical Engineers, New York, NY

ASME Boiler and Pressure Vessel Code, (2025), “Rules for construction of Nuclear Facility Components”, Division 5-High Temperature Reactors, American Society of Mechanical Engineers, New York, NY

Barua, B, Messner, M.C., Sham, T.-L., Jetter, R. I., Wang, Y., (2020), "Preliminary description of a new creep-fatigue design method that reduces over conservatism and simplifies the high temperature design process", ANL-ART-194, Argonne National Laboratory, Lemont, IL.

Barua, B, Messner, M.C., Wang, Y., Sham, T.-L., Jetter, R. I. (2021), "Draft Rules for Alloy 617 Creep-Fatigue Design using an EPP+SMT Approach", ANL-ART-227, Argonne National Laboratory, Lemont, IL

Barua, Bipul and Messner, Mark C. (2024), “ASME Section III, Division 5, Class A 100,000-hour design data for Alloy 709.” Technical report ANL-ART-285, Argonne National Laboratory.

Bhesania, Abhishek and Mark C. Messner. (2025) “ASME Code change proposal to implement new universal high temperature constitutive models for Section III, Division 5.” Technical report ANL-ART-306, Argonne National Laboratory.

Code Case N-898 (2019), ASME BPVC Code Case for Use of Alloy 617 (UNS N06617) for Class A Elevated Temperature Service Construction Section III, Division 5.

Hou, P, Wang, Y. and Sham, T.-L. (2023), “A Method for Evaluation of Creep-Fatigue Life at Low Strain Ranges”, Proceedings of the ASME 2023 Pressure Vessels and Piping Conference, PVP2023-106512, American Society of Mechanical Engineers, Atlanta, Georgia.

Jetter, R. I., (1998), “An Alternate Approach to Evaluation of Creep-Fatigue Damage for High Temperature Structural Design Criteria,” PVP-Vol. 5 Fatigue, Fracture and High Temperature Design Methods in Pressure Vessel and Piping, Book No. H01146 – 1998, American Society of Mechanical Engineers Press, New York, New York.

Kasahara, N., Nagata, T., Iwata, K. and Negishi, H., (1995), “Advanced Creep-Fatigue Evaluation Rule for Fast Breeder Reactor Components: Generalization of Elastic Follow-up Model,” Nuclear Engineering and Design, Vol. 155, pp. 499-518.

Takahura, K., Ueta, M., Dousaki, K. Wada, H., Hayashi, M., Ozaki, H., and Ooka, Y., (1995), "Elevated Temperature Structural Design Guide for DFBR in Japan," Transactions of the 13th International Conference on Structural Mechanics in Reactor Technology, Vol. 1, P380.

Messner, M. C., Sham, T. L., Wang, Y., and Jetter, R.I. (2018), “Evaluation of methods to determine strain ranges for use in SMT design curves”, ANL-ART-138, Argonne National Laboratory, Lemont, IL.

Messner, M.C. and Sham, T.L. (2021). A Viscoplastic Model for Alloy 617 for Use with the ASME Section III, Division 5 Design by Inelastic Analysis Rules. In Pressure Vessels and Piping Conference (Vol. 85314, p. V001T01A034). American Society of Mechanical Engineers.

Messner, M. C., Jetter. B, and Sham, T. L. (2019), “A Method for Directly Assessing Elastic Follow Up in 3D Finite Element Calculations,” Proceedings of the ASME 2019 Pressure Vessels & Piping Conference, PVP2019-93644, American Society of Mechanical Engineers, New York.

Wang, Y., Jetter, R. I. and Sham, T.-L (2014), “Application of Combined Sustained and Cyclic Loading Test Results to Alloy 617 Elevated Temperature Design Criteria”, ORNL/TM-2014/294, Oak Ridge National Laboratory, Oak Ridge, TN.

Wang, Y., Jetter, R. I., and Sham, T.-L. (2016a), "FY16 Progress Report on Test Results In Support Of Integrated EPP and SMT Design Methods Development" ORNL/TM-2016/330, Oak Ridge National Laboratory, Oak Ridge, TN.

Wang, Y., Jetter, R. I., and Sham, T.-L. (2016b), "Preliminary Test Results in Support of Integrated EPP and SMT Design Methods Development", ORNL/TM-2016/76, Oak Ridge National Laboratory, Oak Ridge, TN.

Wang, Y., Jetter, R.I., and Sham, T.-L. (2017a), "Report on FY17 Testing in Support of Integrated EPP-SMT Design Methods Development", ORNL/TM-2017/351, Oak Ridge National Laboratory, Oak Ridge, TN.

Wang, Y., Jetter, and Sham, T.-L. (2017b), "Pressurized Creep-Fatigue Testing of Alloy 617 Using Simplified Model Test Method", Proceedings of the ASME 2017 Pressure Vessels and Piping Conference, PVP2017-65457, American Society of Mechanical Engineers, New York, NY.

Wang, Y., Jetter, R. I., Messner, M., and Sham, T.-L. (2018), "Report on FY18 Testing Results in Support of Integrated EPP-SMT Design Methods Development", ORNL/TM-2018/887, Oak Ridge National Laboratory, Oak Ridge, TN.

Wang, Y., Jetter, R. I., Messner, M., and Sham, T.-L. (2019), "Development of Simplified Model Test Method for Creep-fatigue Evaluation", Proceedings of the ASME 2019 Pressure Vessels and Piping Conference, PVP2019-93648, American Society of Mechanical Engineers, New York, NY.

Wang, Yanli, et al. "Effect of Internal Pressurization on the Creep-Fatigue Performance of Alloy 617 Based on Simplified Model Test Method." In the proceedings of the 2019 ASME Pressure Vessels & Piping Conference, 2019.

Wang, Y., Hou, P., Jetter, R. I., and Sham, T.-L. (2020), "Report on FY2020 Test Results in Support of the Development of EPP Plus SMT Design Method", ORNL/TM-2020/1620, Oak Ridge National Laboratory, Oak Ridge, TN.

Wang, Y., Hou, P., Jetter, R. I., and Sham, T.-L. (2021a), "Evaluation of the Primary-Load Effects on Creep-Fatigue Life of Alloy 617 Using Simplified Model Test Method", Proceedings of the ASME 2021 Pressure Vessels and Piping Conference, PVP2021-61658, American Society of Mechanical Engineers, New York, NY

Wang, Y., Hou, P., Jetter, R. I., and Sham, T.-L. (2021b), "Report on FY2021 Test Results in Support of the Development of EPP Plus SMT Design Method", ORNL/TM-2021/2159, Oak Ridge National Laboratory, Oak Ridge, TN.

Wang, Y. (2024), "New ASME Section III, Division 5 Creep-Fatigue Design Rules Based on EPP and SMT Approaches", ORNL/TM-2024/ 3611, Oak Ridge National Laboratory, Oak Ridge, TN.

Wright, R. N. (2021). "Draft ASME Boiler and Pressure Vessel Code Cases and Technical Bases for Use of Alloy 617 for Construction of Nuclear Components Under Section Ill, Division 5". INL/EXT-15-36305, Idaho National Laboratory, Idaho Falls, Idaho.

APPENDIX A.

This Appendix plots the inelastic model predictions for the stress-strain hysteresis and the amount of work dissipated by the material as a function of cycle count versus the test data for all 70 experiments. The figures all have the same format:

- Each row represents a separate test. The subfigure on the left shows the amount of work dissipated per cycle with the test data in black, the median model prediction as a blue line, and the model 90% prediction interval as a shaded blue region.
- The subfigure on the right shows the experimental stress-strain hysteresis, the median model prediction, and the model 90% prediction interval in the same color scheme.
  The temperature values shown in the figures are consistent with the average test temperatures recorded during the experiment.

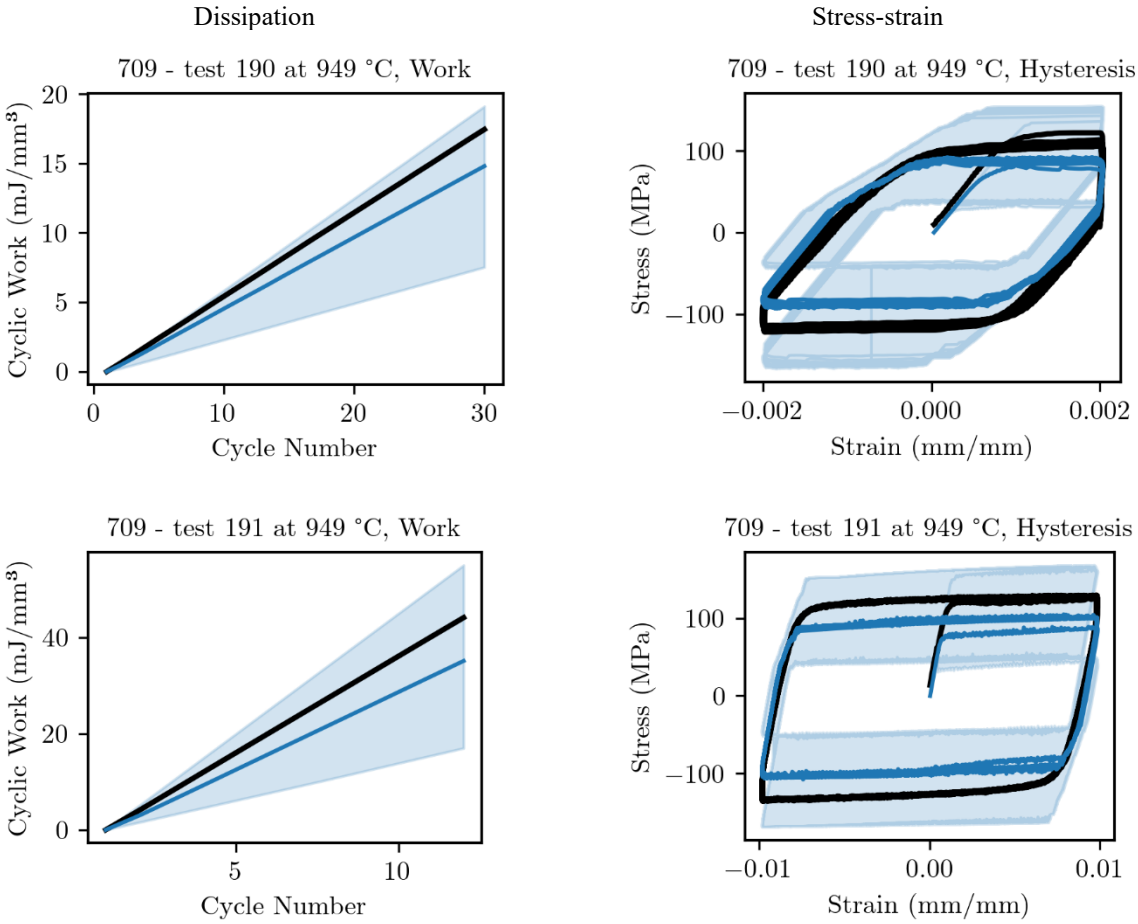

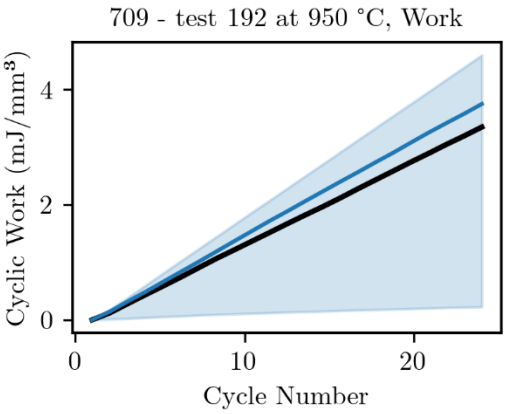
709 - test 192 at 950 °C, Work
Cyclic Work (mJ/mm³)
0
2
4
0
10
20
Cycle Number

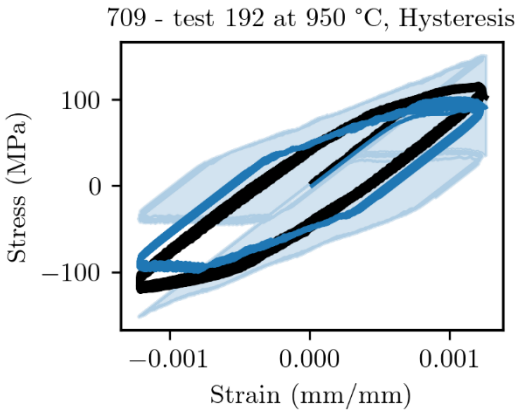
709 - test 192 at 950 °C, Hysteresis
Stress (MPa)
100
0
−100
−0.001
0.000
0.001
Strain (mm/mm)

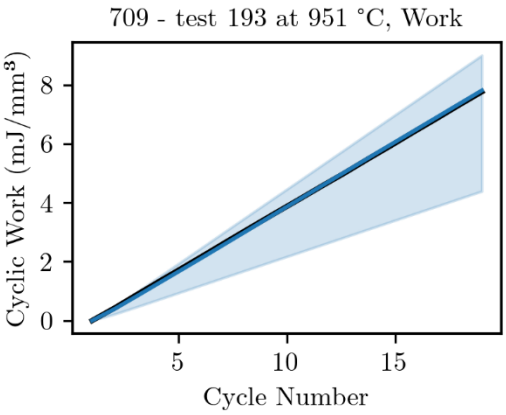
709 - test 193 at 951 °C, Work
Cyclic Work (mJ/mm³)
0
2
4
6
8
5
10
15
Cycle Number

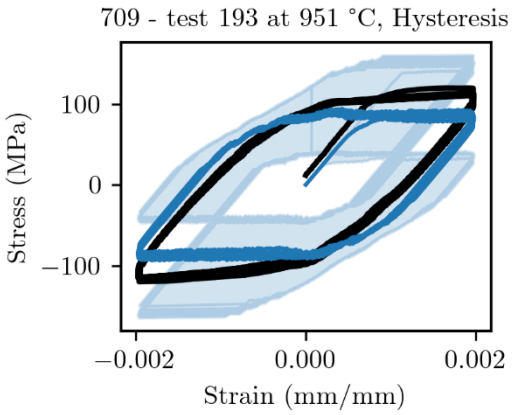
709 - test 193 at 951 °C, Hysteresis
Stress (MPa)
100
0
−100
−0.002
0.000
0.002
Strain (mm/mm)

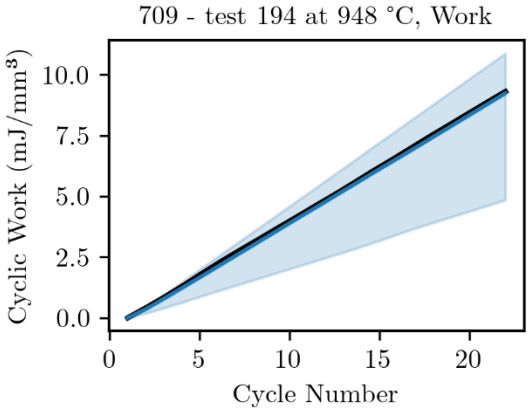
709 - test 194 at 948 °C, Work
Cyclic Work (mJ/mm³)
0.0
2.5
5.0
7.5
10.0
0
5
10
15
20
Cycle Number

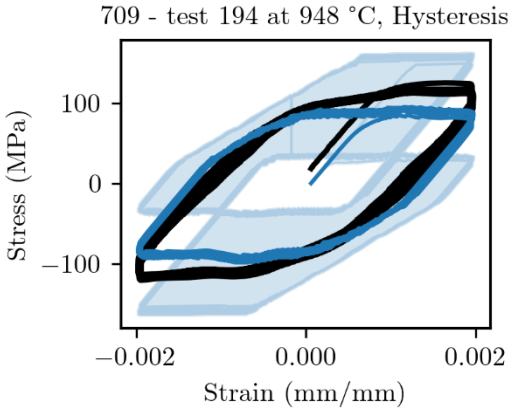
709 - test 194 at 948 °C, Hysteresis
Stress (MPa)
100
0
−100
−0.002
0.000
0.002
Strain (mm/mm)

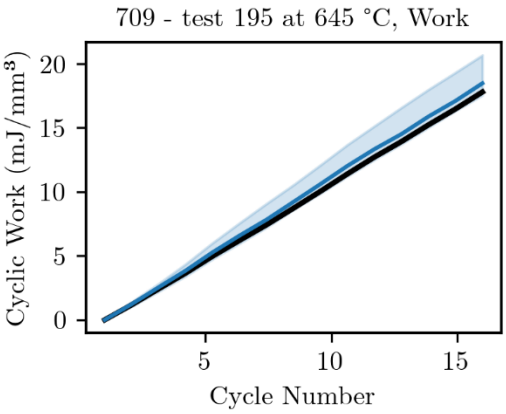
709 - test 195 at 645 °C, Work
Cyclic Work (mJ/mm³)
0
5
10
15
20
5
10
15
Cycle Number

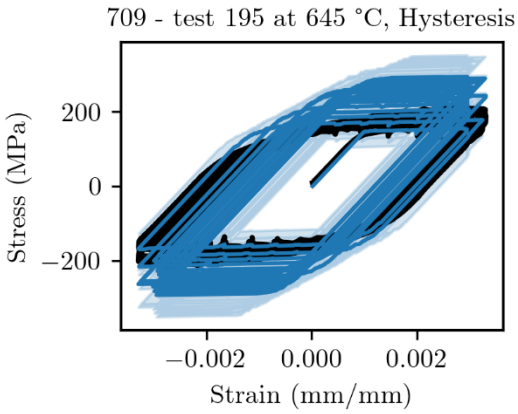
709 - test 195 at 645 °C, Hysteresis
Stress (MPa)
−200
0
200
−0.002
0.000
0.002
Strain (mm/mm)

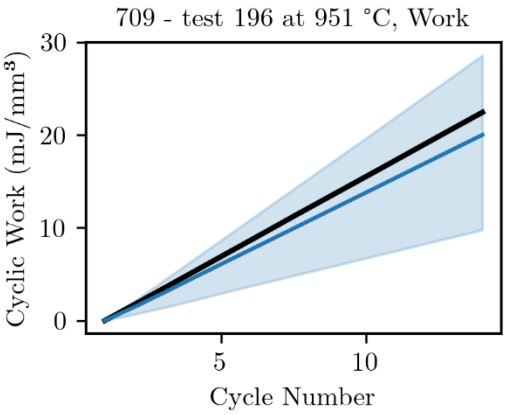
709 - test 196 at 951 °C, Work
Cyclic Work (mJ/mm³)
0
10
20
30
5
10
Cycle Number

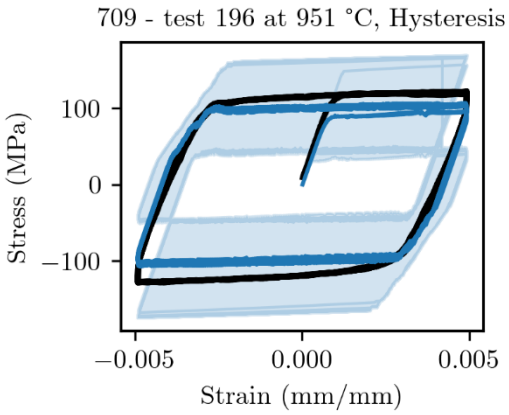
709 - test 196 at 951 °C, Hysteresis
Stress (MPa)
−100
0
100
−0.005
0.000
0.005
Strain (mm/mm)

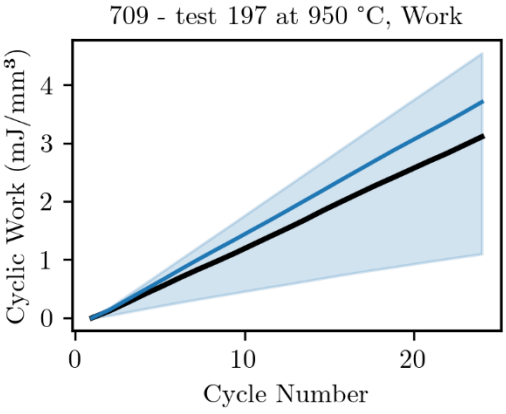
709 - test 197 at 950 °C, Work
Cyclic Work (mJ/mm³)
0
1
2
3
4
0
10
20
Cycle Number

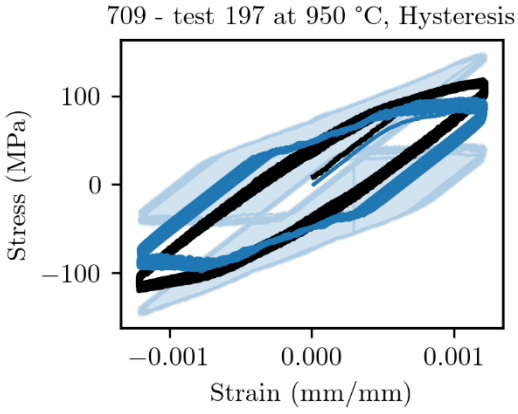
709 - test 197 at 950 °C, Hysteresis
Stress (MPa)
−100
0
100
−0.001
0.000
0.001
Strain (mm/mm)

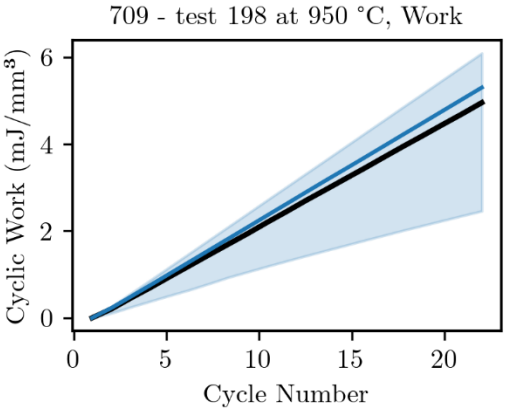
709 - test 198 at 950 °C, Work
Cyclic Work (mJ/mm³)
Cycle Number

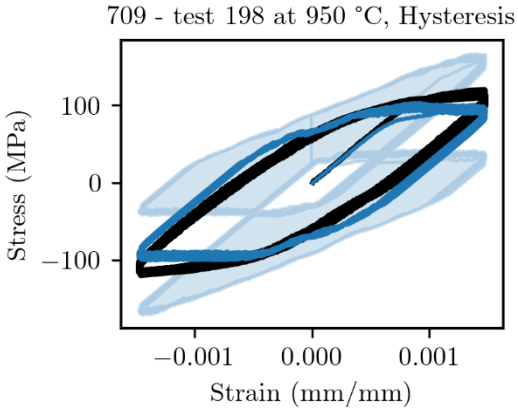
709 - test 198 at 950 °C, Hysteresis
Stress (MPa)
Strain (mm/mm)

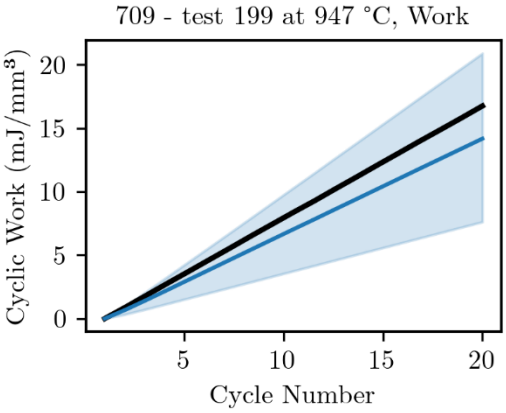
709 - test 199 at 947 °C, Work
Cyclic Work (mJ/mm³)
Cycle Number

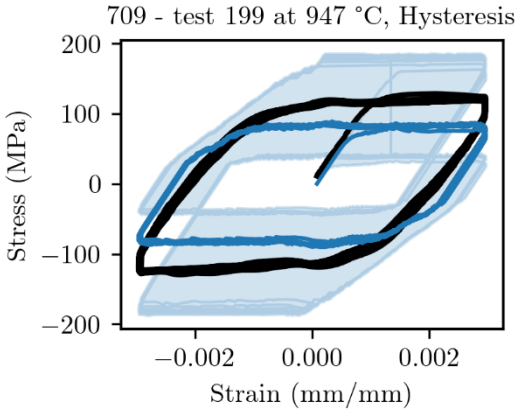
709 - test 199 at 947 °C, Hysteresis
Stress (MPa)
Strain (mm/mm)

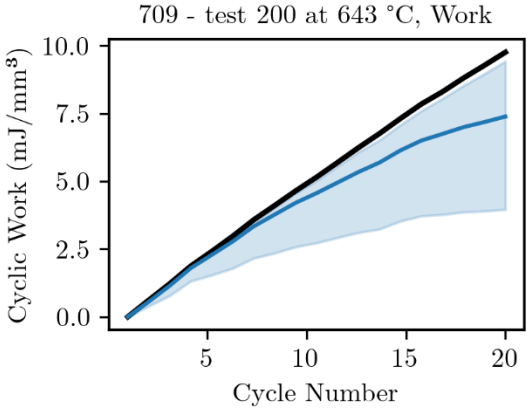
709 - test 200 at 643 °C, Work
Cyclic Work (mJ/mm³)
Cycle Number

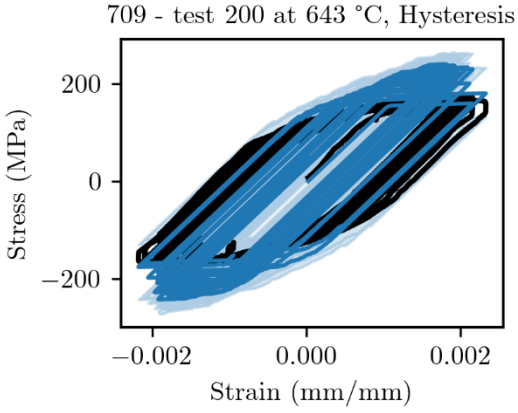
709 - test 200 at 643 °C, Hysteresis
Stress (MPa)
Strain (mm/mm)

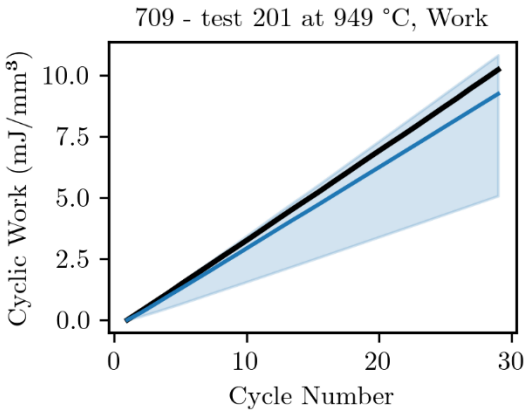
709 - test 201 at 949 °C, Work
Cyclic Work (mJ/mm³)
10.0
7.5
5.0
2.5
0.0
0
10
20
30
Cycle Number

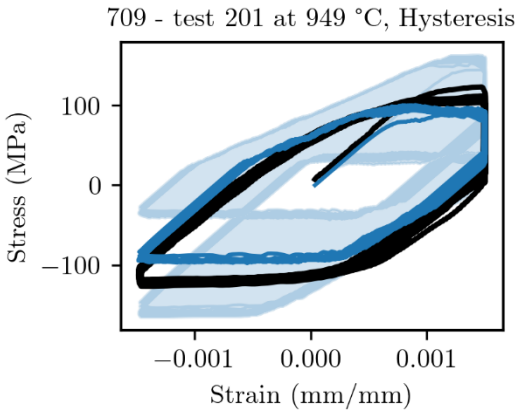
709 - test 201 at 949 °C, Hysteresis
Stress (MPa)
100
0
−100
−0.001
0.000
0.001
Strain (mm/mm)

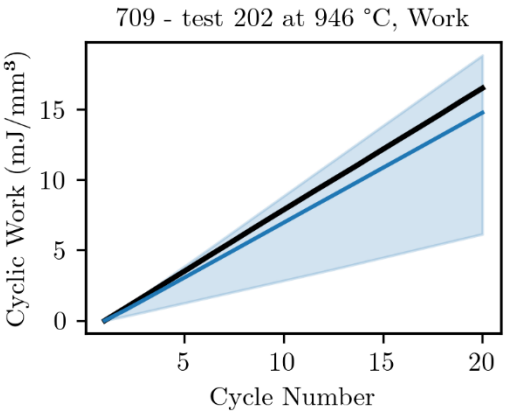
709 - test 202 at 946 °C, Work
Cyclic Work (mJ/mm³)
15
10
5
0
5
10
15
20
Cycle Number

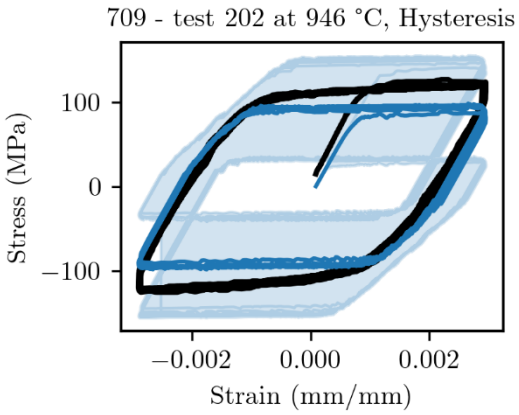
709 - test 202 at 946 °C, Hysteresis
Stress (MPa)
100
0
−100
−0.002
0.000
0.002
Strain (mm/mm)

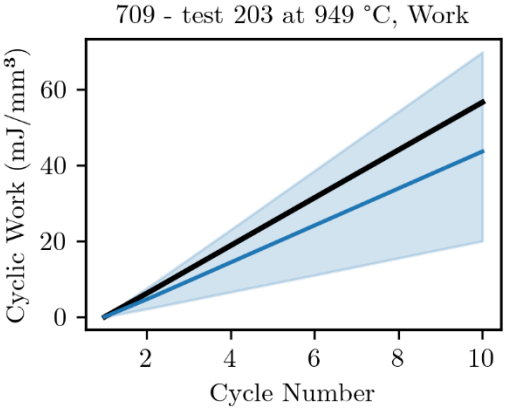
709 - test 203 at 949 °C, Work
Cyclic Work (mJ/mm³)
60
40
20
0
2
4
6
8
10
Cycle Number

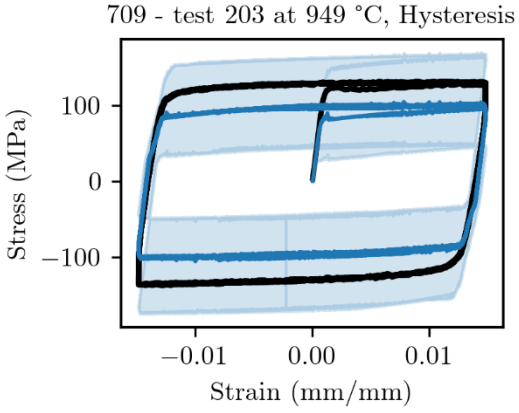
709 - test 203 at 949 °C, Hysteresis
Stress (MPa)
100
0
−100
−0.01
0.00
0.01
Strain (mm/mm)

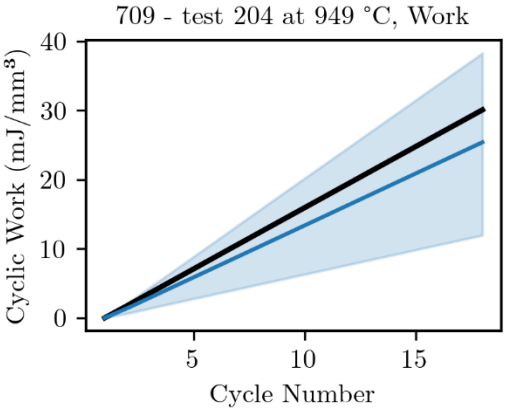
709 - test 204 at 949 °C, Work
Cyclic Work (mJ/mm³)
0
10
20
30
40
5
10
15
Cycle Number

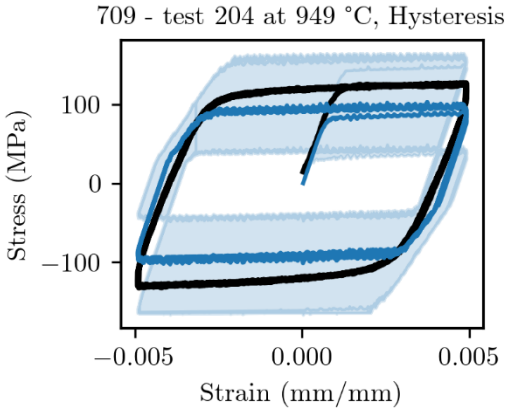
709 - test 204 at 949 °C, Hysteresis
Stress (MPa)
−100
0
100
−0.005
0.000
0.005
Strain (mm/mm)

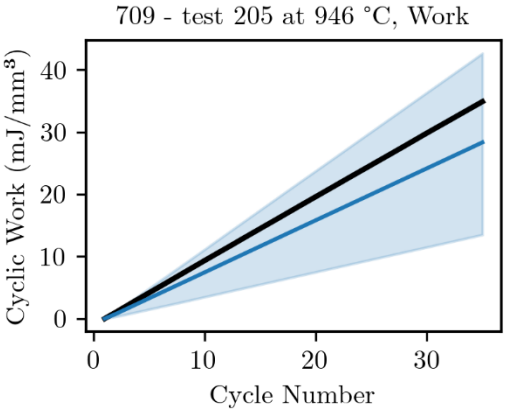
709 - test 205 at 946 °C, Work
Cyclic Work (mJ/mm³)
0
10
20
30
40
0
10
20
30
Cycle Number

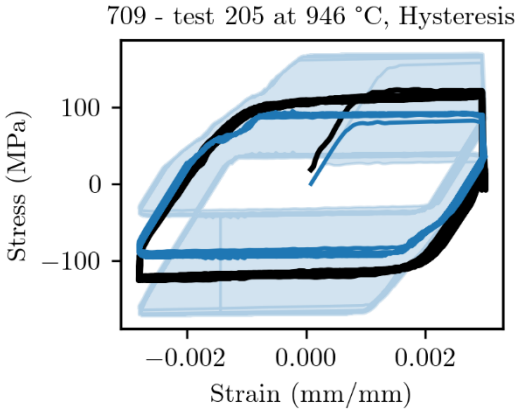
709 - test 205 at 946 °C, Hysteresis
Stress (MPa)
−100
0
100
−0.002
0.000
0.002
Strain (mm/mm)

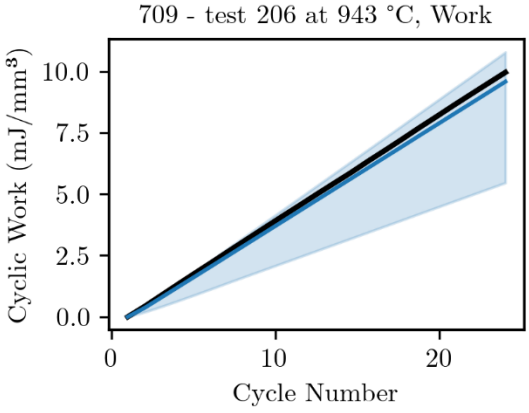
709 - test 206 at 943 °C, Work
Cyclic Work (mJ/mm³)
0.0
2.5
5.0
7.5
10.0
0
10
20
Cycle Number

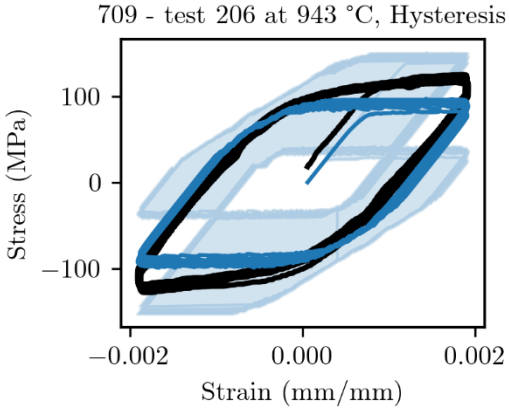
709 - test 206 at 943 °C, Hysteresis
Stress (MPa)
−100
0
100
−0.002
0.000
0.002
Strain (mm/mm)

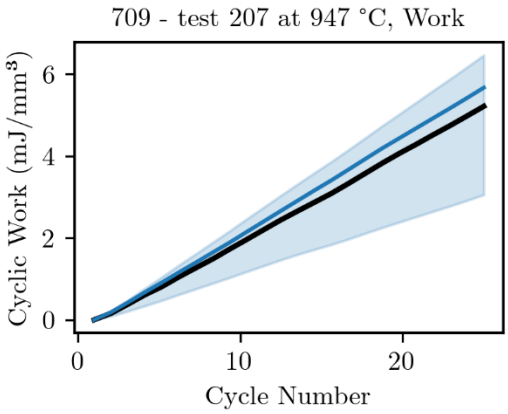
709 - test 207 at 947 °C, Work
Cyclic Work (mJ/mm³)
0
2
4
6
0
10
20
Cycle Number

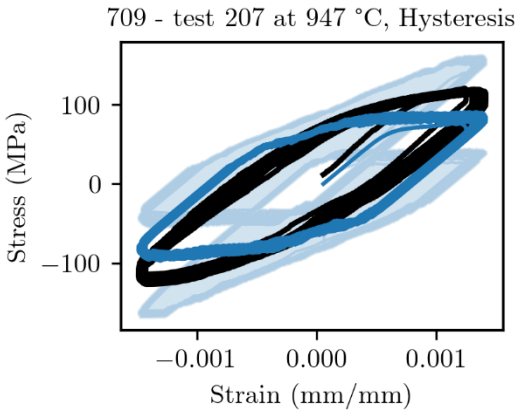
709 - test 207 at 947 °C, Hysteresis
Stress (MPa)
−100
0
100
−0.001
0.000
0.001
Strain (mm/mm)

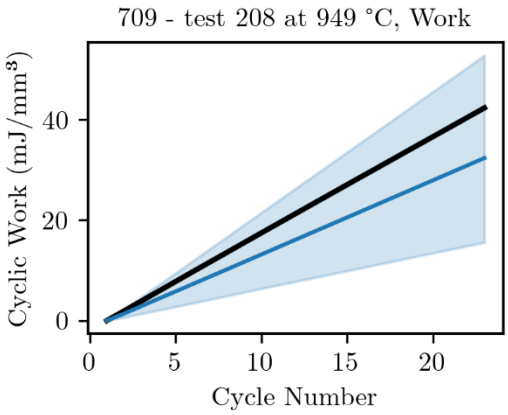
709 - test 208 at 949 °C, Work
Cyclic Work (mJ/mm³)
0
20
40
0
5
10
15
20
Cycle Number

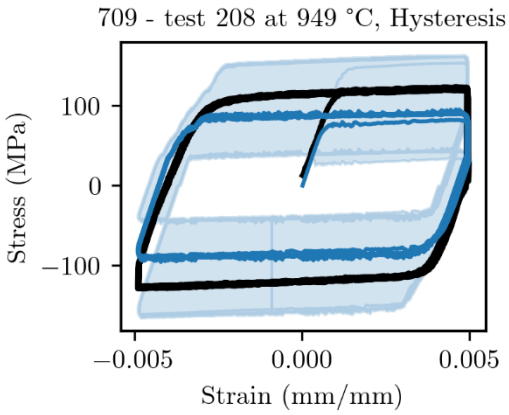
709 - test 208 at 949 °C, Hysteresis
Stress (MPa)
−100
0
100
−0.005
0.000
0.005
Strain (mm/mm)

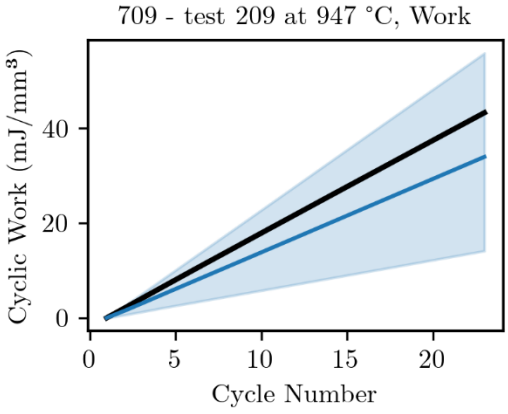
709 - test 209 at 947 °C, Work
Cyclic Work (mJ/mm³)
0
20
40
0
5
10
15
20
Cycle Number

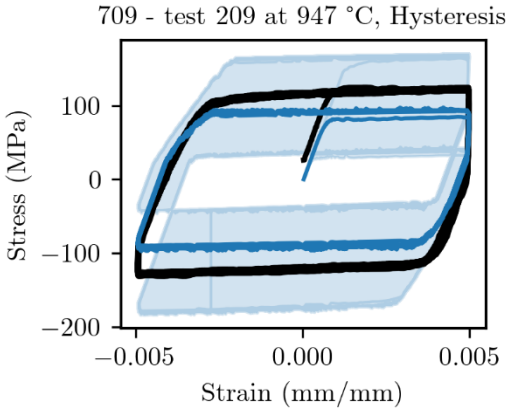
709 - test 209 at 947 °C, Hysteresis
Stress (MPa)
−200
−100
0
100
−0.005
0.000
0.005
Strain (mm/mm)

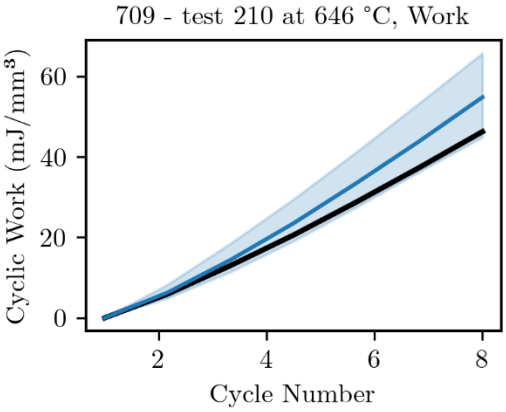
709 - test 210 at 646 °C, Work
Cyclic Work (mJ/mm³)
0
20
40
60
2
4
6
8
Cycle Number

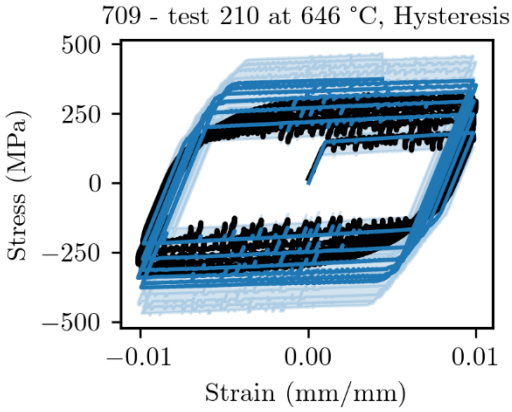
709 - test 210 at 646 °C, Hysteresis
Stress (MPa)
−500
−250
0
250
500
−0.01
0.00
0.01
Strain (mm/mm)

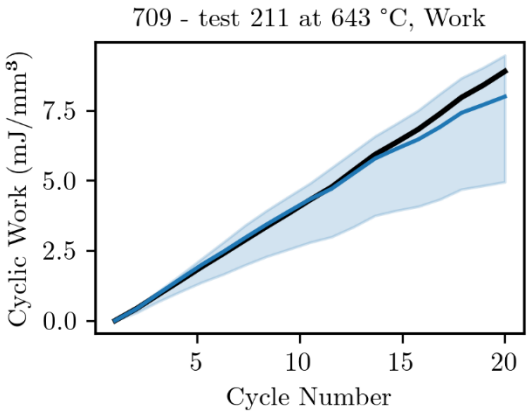
709 - test 211 at 643 °C, Work
Cyclic Work (mJ/mm³)
0.0
2.5
5.0
7.5
5
10
15
20
Cycle Number

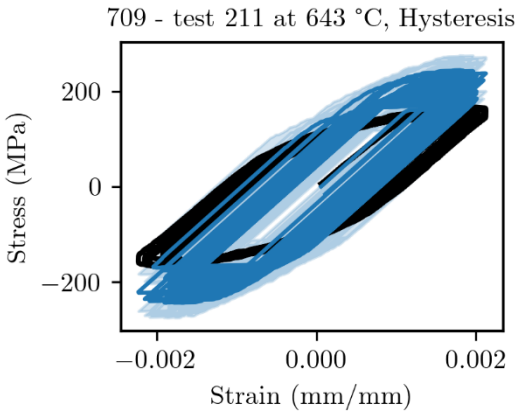
709 - test 211 at 643 °C, Hysteresis
Stress (MPa)
−200
0
200
−0.002
0.000
0.002
Strain (mm/mm)

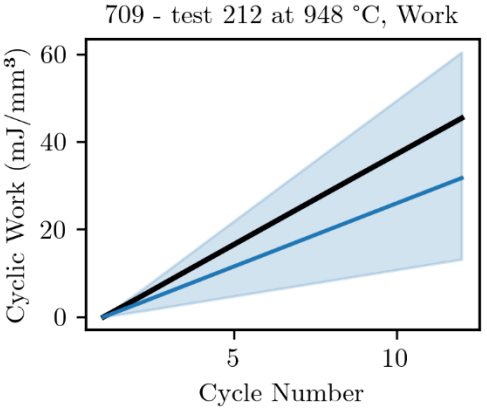
709 - test 212 at 948 °C, Work
Cyclic Work (mJ/mm³)
0
20
40
60
5
10
Cycle Number

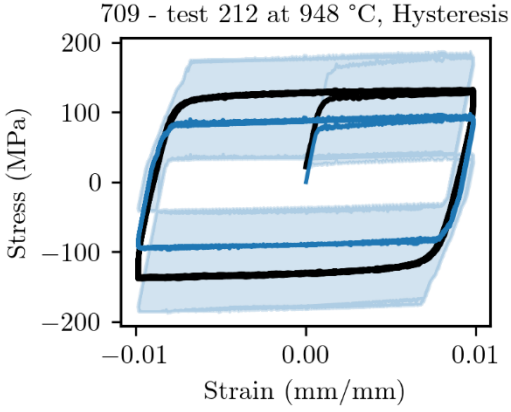
709 - test 212 at 948 °C, Hysteresis
Stress (MPa)
−200
−100
0
100
200
−0.01
0.00
0.01
Strain (mm/mm)

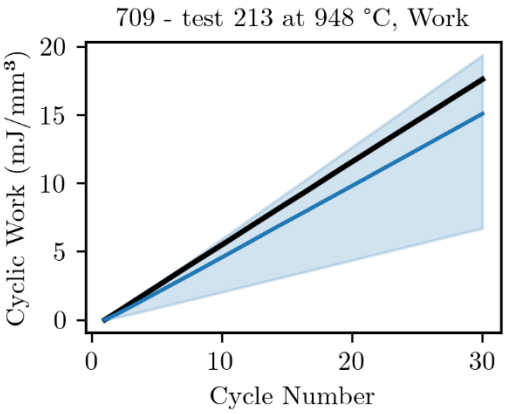
709 - test 213 at 948 °C, Work
Cyclic Work (mJ/mm³)
0
5
10
15
20
0
10
20
30
Cycle Number

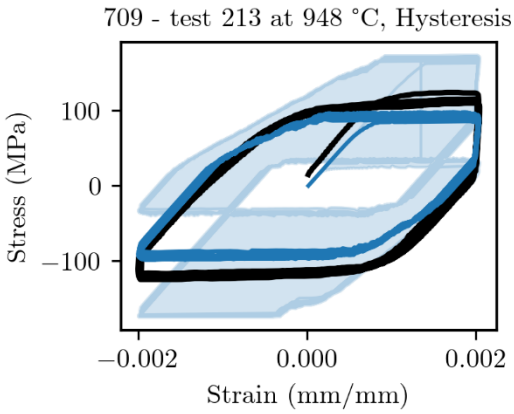
709 - test 213 at 948 °C, Hysteresis
Stress (MPa)
−100
0
100
−0.002
0.000
0.002
Strain (mm/mm)

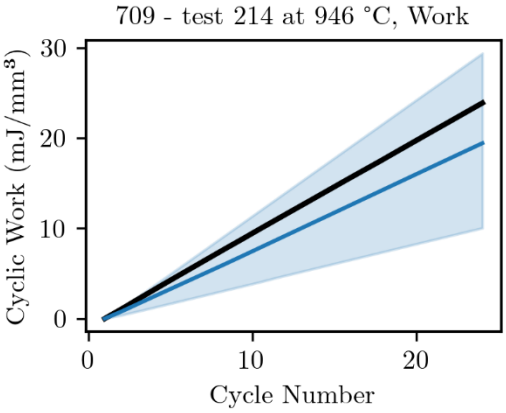
709 - test 214 at 946 °C, Work
Cyclic Work (mJ/mm³)
0
10
20
30
0
10
20
Cycle Number

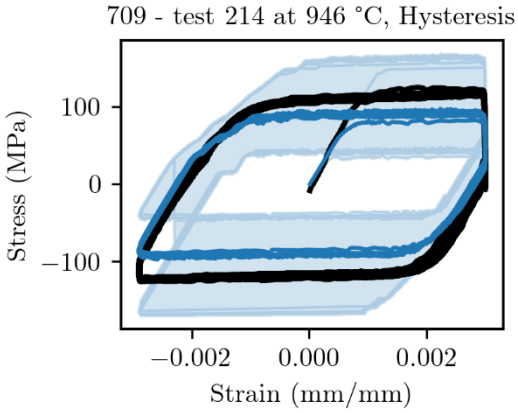
709 - test 214 at 946 °C, Hysteresis
Stress (MPa)
−100
0
100
−0.002
0.000
0.002
Strain (mm/mm)

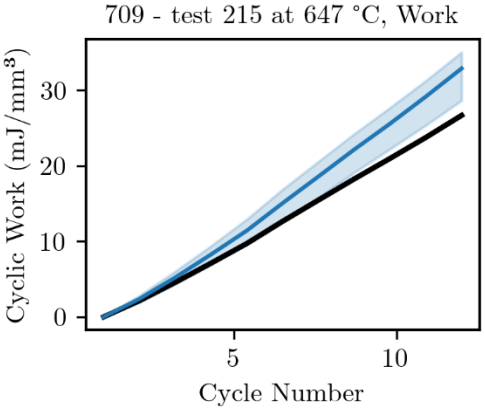
709 - test 215 at 647 °C, Work
Cyclic Work (mJ/mm³)
0
10
20
30
5
10
Cycle Number

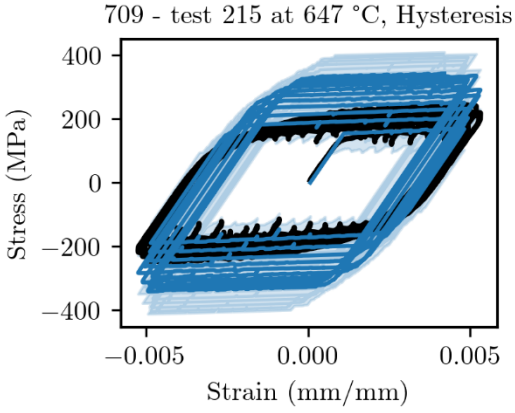
709 - test 215 at 647 °C, Hysteresis
Stress (MPa)
−400
−200
0
200
400
−0.005
0.000
0.005
Strain (mm/mm)

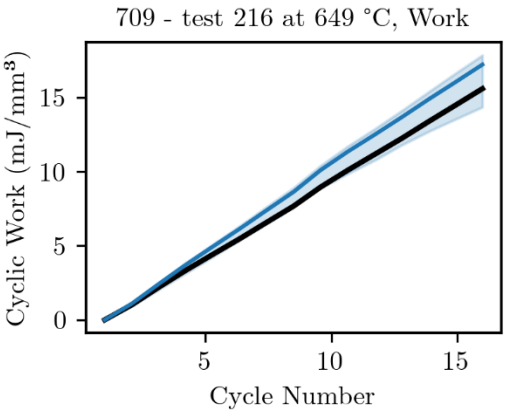
709 - test 216 at 649 °C, Work
Cyclic Work (mJ/mm³)
0
5
10
15
5
10
15
Cycle Number

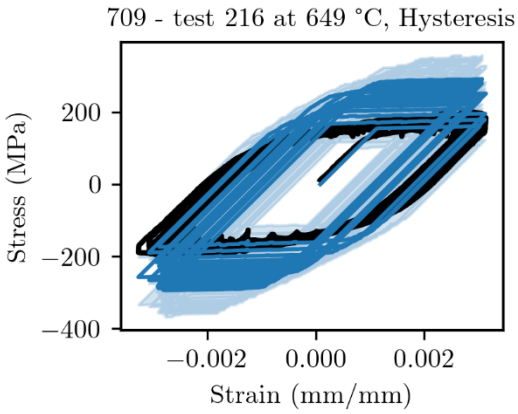
709 - test 216 at 649 °C, Hysteresis
Stress (MPa)
200
0
−200
−400
−0.002
0.000
0.002
Strain (mm/mm)

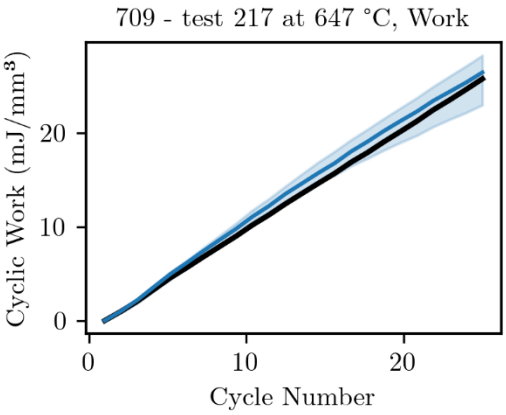
709 - test 217 at 647 °C, Work
Cyclic Work (mJ/mm³)
0
10
20
0
10
20
Cycle Number

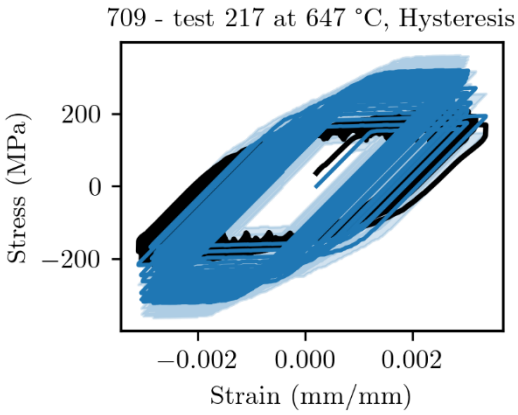
709 - test 217 at 647 °C, Hysteresis
Stress (MPa)
200
0
−200
−0.002
0.000
0.002
Strain (mm/mm)

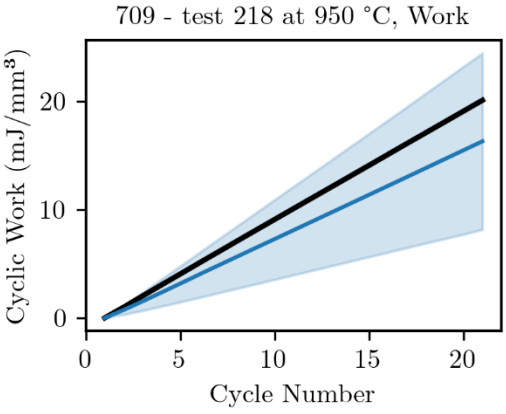
709 - test 218 at 950 °C, Work
Cyclic Work (mJ/mm³)
0
10
20
0
5
10
15
20
Cycle Number

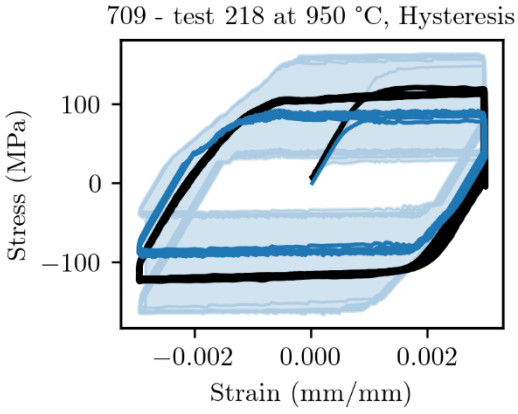
709 - test 218 at 950 °C, Hysteresis
Stress (MPa)
100
0
−100
−0.002
0.000
0.002
Strain (mm/mm)

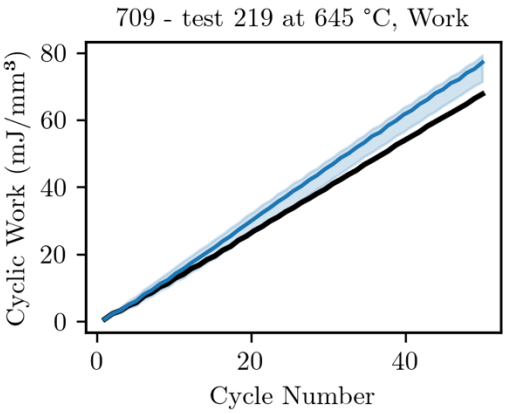
709 - test 219 at 645 °C, Work
Cyclic Work (mJ/mm³)
0
20
40
60
80
0
20
40
Cycle Number

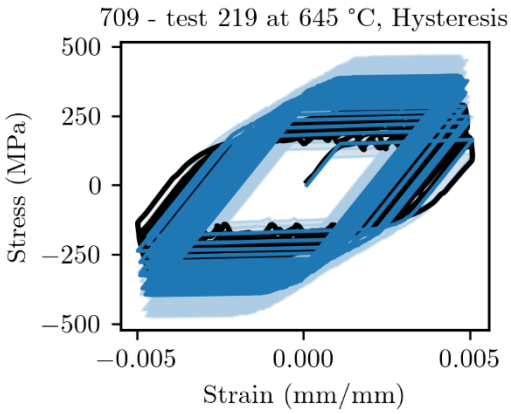
709 - test 219 at 645 °C, Hysteresis
Stress (MPa)
500
250
0
−250
−500
−0.005
0.000
0.005
Strain (mm/mm)

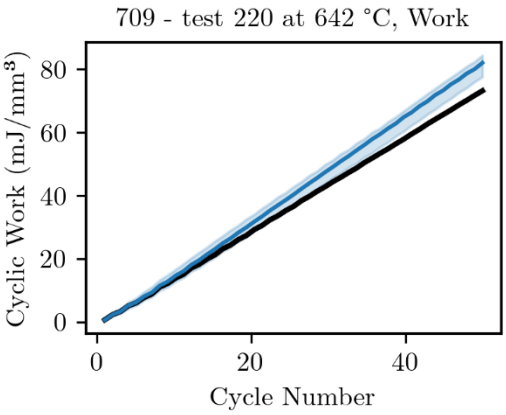
709 - test 220 at 642 °C, Work
Cyclic Work (mJ/mm³)
0
20
40
60
80
0
20
40
Cycle Number

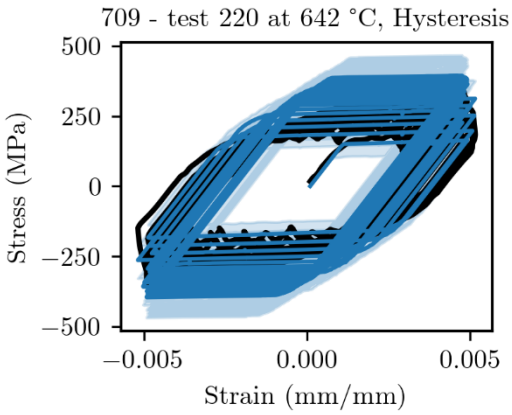
709 - test 220 at 642 °C, Hysteresis
Stress (MPa)
500
250
0
−250
−500
−0.005
0.000
0.005
Strain (mm/mm)

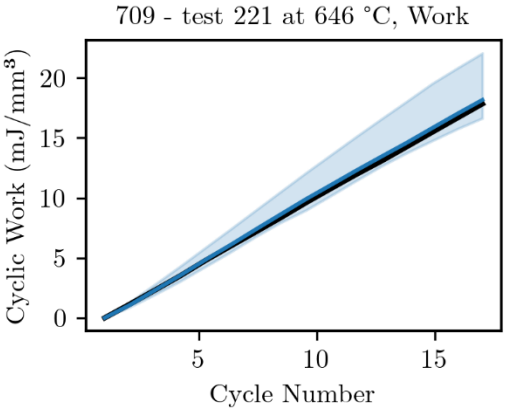
709 - test 221 at 646 °C, Work
Cyclic Work (mJ/mm³)
0
5
10
15
20
5
10
15
Cycle Number

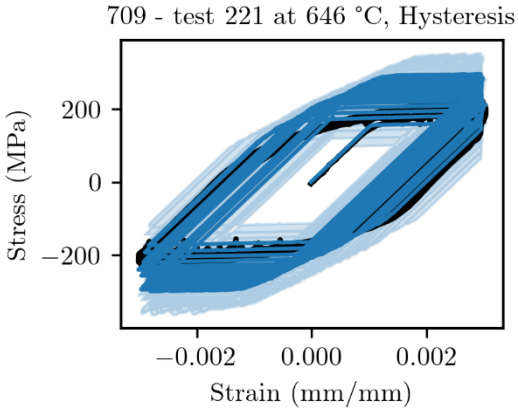
709 - test 221 at 646 °C, Hysteresis
Stress (MPa)
200
0
−200
−0.002
0.000
0.002
Strain (mm/mm)

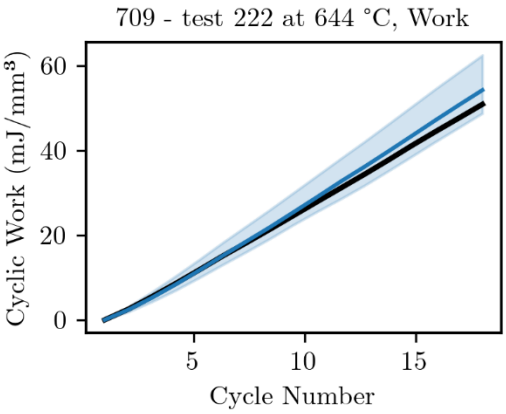
709 - test 222 at 644 °C, Work
Cyclic Work (mJ/mm³)
0
20
40
60
5
10
15
Cycle Number

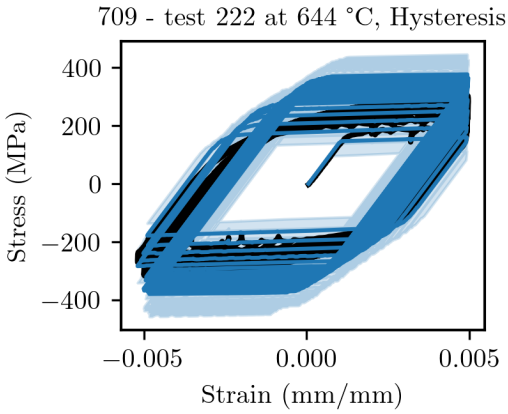
709 - test 222 at 644 °C, Hysteresis
Stress (MPa)
−400
−200
0
200
400
−0.005
0.000
0.005
Strain (mm/mm)

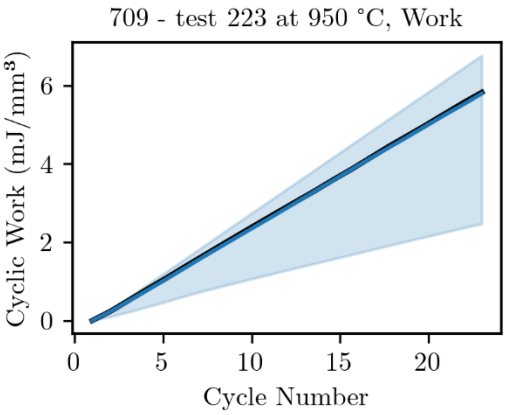
709 - test 223 at 950 °C, Work
Cyclic Work (mJ/mm³)
0
2
4
6
0
5
10
15
20
Cycle Number

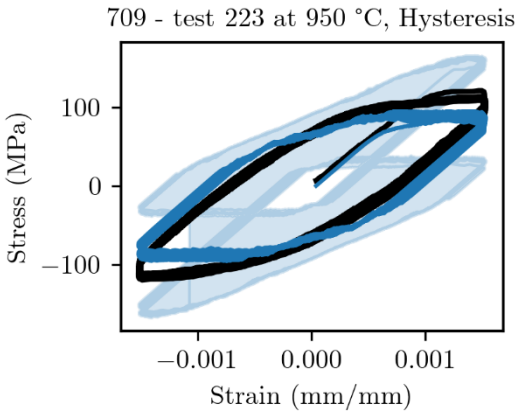
709 - test 223 at 950 °C, Hysteresis
Stress (MPa)
−100
0
100
−0.001
0.000
0.001
Strain (mm/mm)

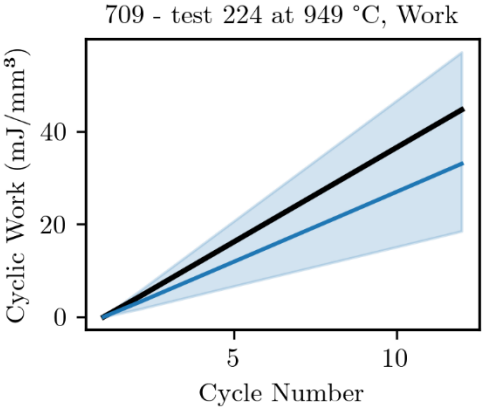
709 - test 224 at 949 °C, Work
Cyclic Work (mJ/mm³)
0
20
40
5
10
Cycle Number

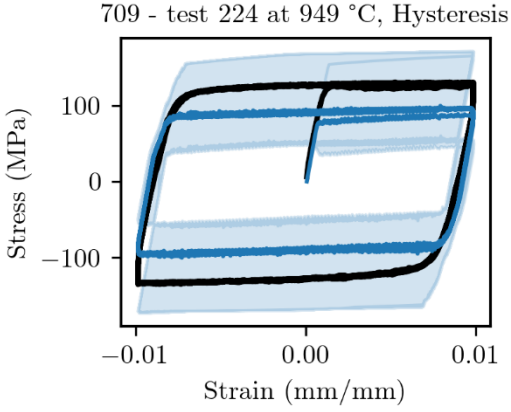
709 - test 224 at 949 °C, Hysteresis
Stress (MPa)
−100
0
100
−0.01
0.00
0.01
Strain (mm/mm)

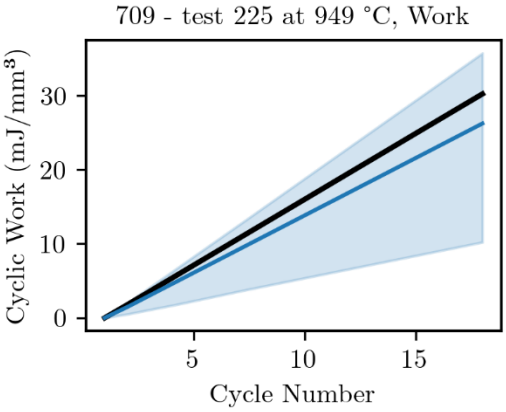
709 - test 225 at 949 °C, Work
Cyclic Work (mJ/mm³)
0
10
20
30
5
10
15
Cycle Number

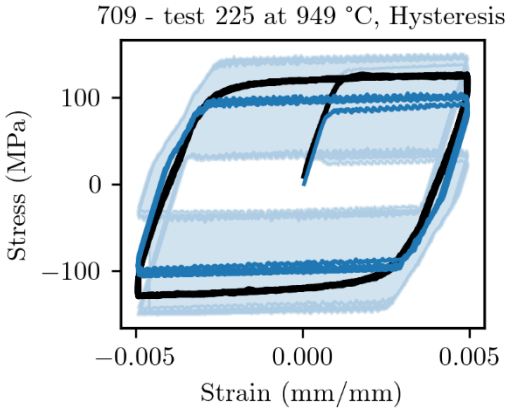
709 - test 225 at 949 °C, Hysteresis
Stress (MPa)
100
0
−100
−0.005
0.000
0.005
Strain (mm/mm)

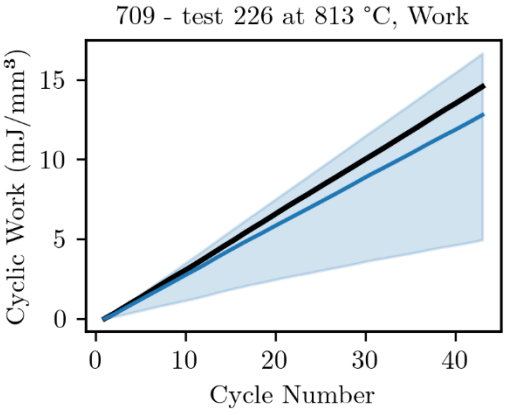
709 - test 226 at 813 °C, Work
Cyclic Work (mJ/mm³)
0
5
10
15
0
10
20
30
40
Cycle Number

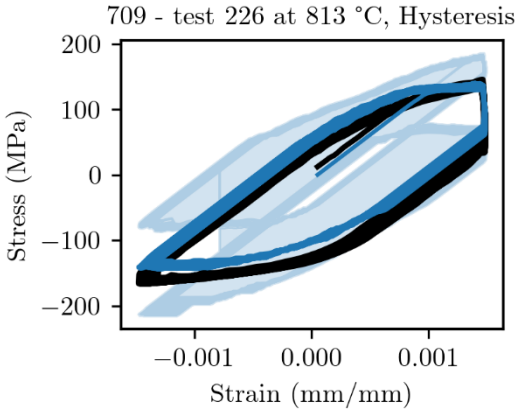
709 - test 226 at 813 °C, Hysteresis
Stress (MPa)
200
100
0
−100
−200
−0.001
0.000
0.001
Strain (mm/mm)

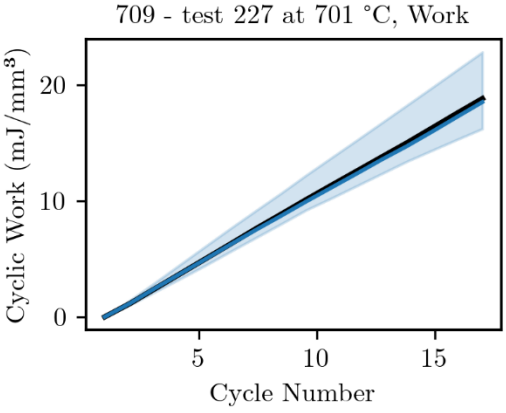
709 - test 227 at 701 °C, Work
Cyclic Work (mJ/mm³)
0
10
20
5
10
15
Cycle Number

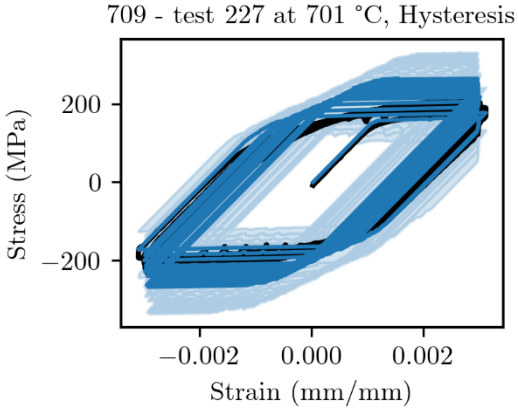
709 - test 227 at 701 °C, Hysteresis
Stress (MPa)
200
0
−200
−0.002
0.000
0.002
Strain (mm/mm)

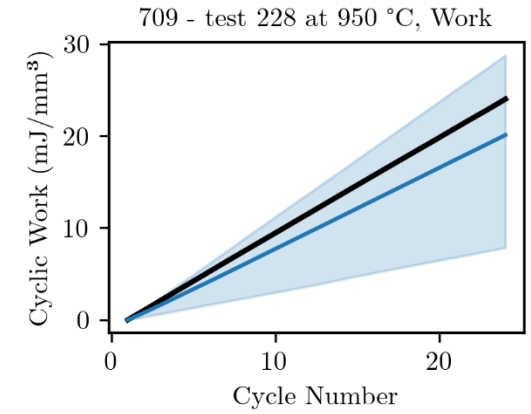
709 - test 228 at 950 °C, Work
Cyclic Work (mJ/mm³)
30
20
10
0
0
10
20
Cycle Number

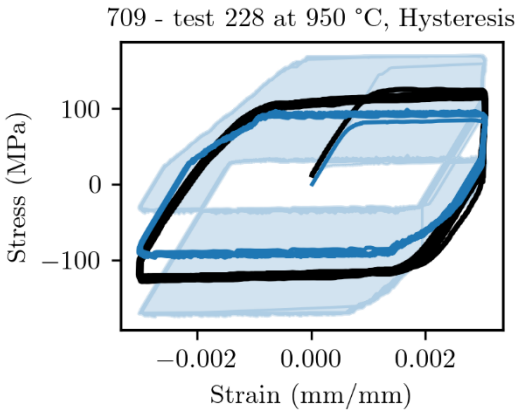
709 - test 228 at 950 °C, Hysteresis
Stress (MPa)
100
0
−100
−0.002
0.000
0.002
Strain (mm/mm)

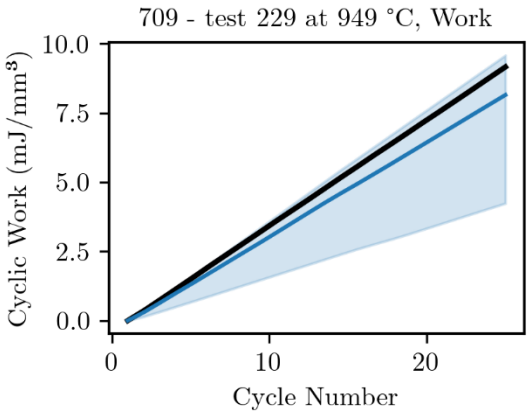
709 - test 229 at 949 °C, Work
Cyclic Work (mJ/mm³)
10.0
7.5
5.0
2.5
0.0
0
10
20
Cycle Number

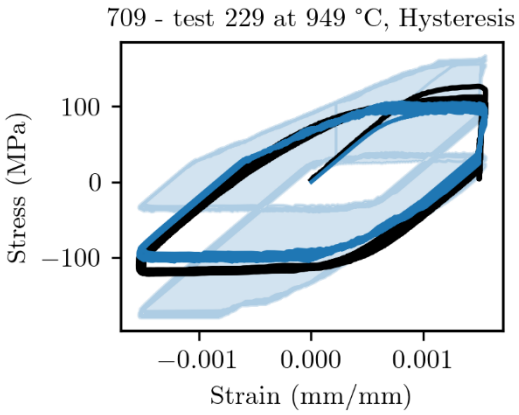
709 - test 229 at 949 °C, Hysteresis
Stress (MPa)
100
0
−100
−0.001
0.000
0.001
Strain (mm/mm)

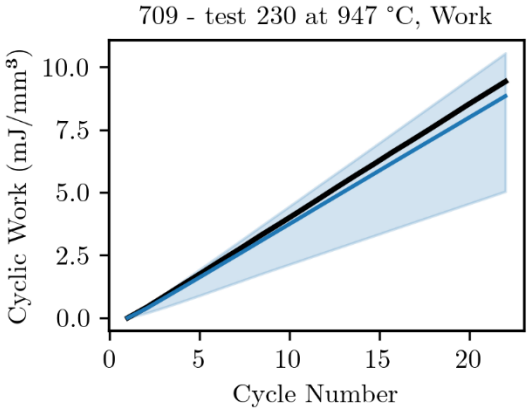
709 - test 230 at 947 °C, Work
Cyclic Work (mJ/mm³)
10.0
7.5
5.0
2.5
0.0
0
5
10
15
20
Cycle Number

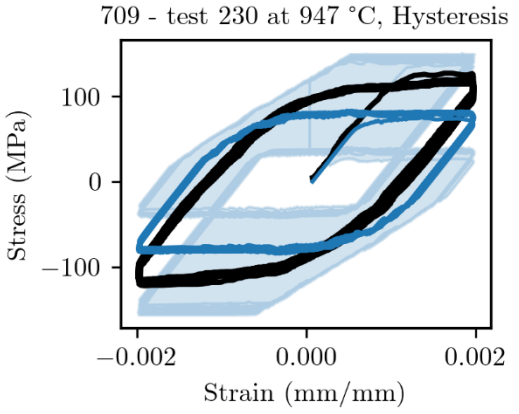
709 - test 230 at 947 °C, Hysteresis
Stress (MPa)
100
0
−100
−0.002
0.000
0.002
Strain (mm/mm)

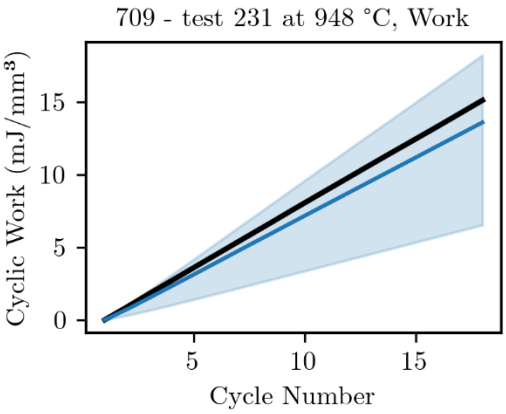
709 - test 231 at 948 °C, Work
Cyclic Work (mJ/mm³)
0
5
10
15
5
10
15
Cycle Number

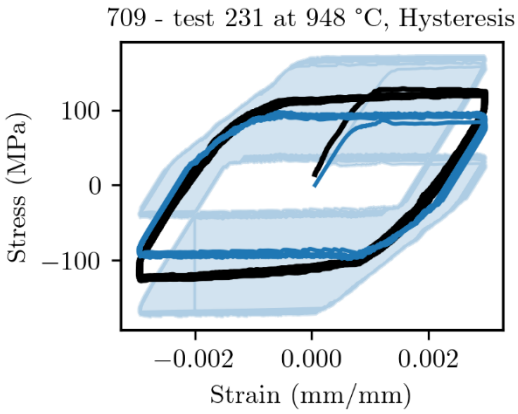
709 - test 231 at 948 °C, Hysteresis
Stress (MPa)
100
0
−100
−0.002
0.000
0.002
Strain (mm/mm)

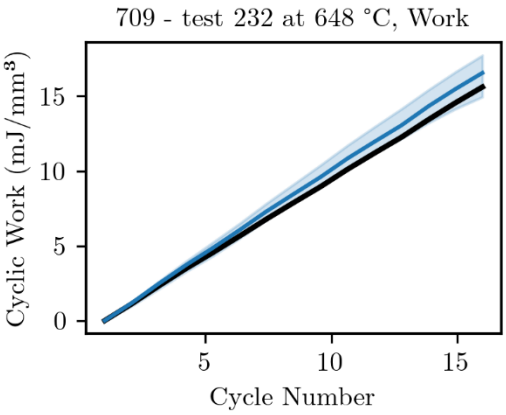
709 - test 232 at 648 °C, Work
Cyclic Work (mJ/mm³)
0
5
10
15
5
10
15
Cycle Number

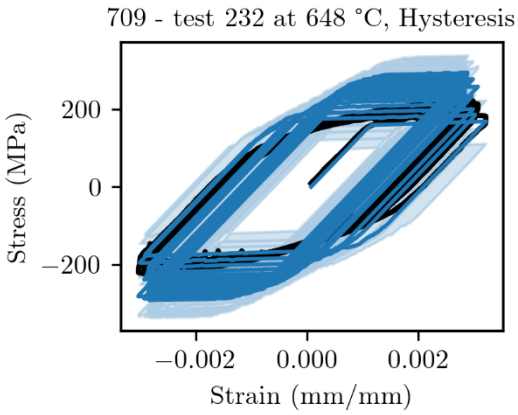
709 - test 232 at 648 °C, Hysteresis
Stress (MPa)
200
0
−200
−0.002
0.000
0.002
Strain (mm/mm)

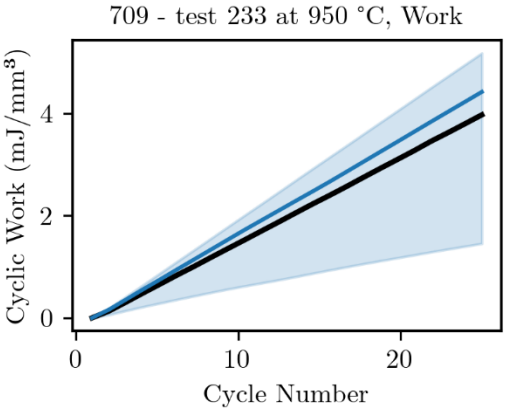
709 - test 233 at 950 °C, Work
Cyclic Work (mJ/mm³)
0
2
4
0
10
20
Cycle Number

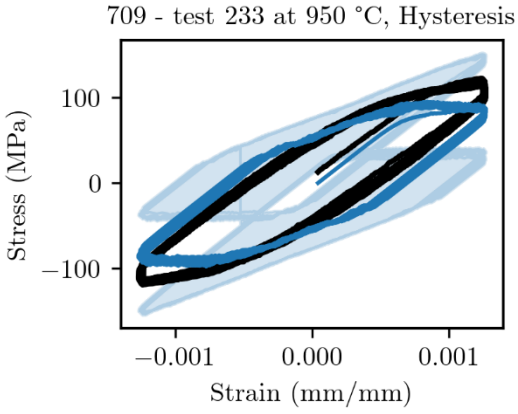
709 - test 233 at 950 °C, Hysteresis
Stress (MPa)
100
0
−100
−0.001
0.000
0.001
Strain (mm/mm)

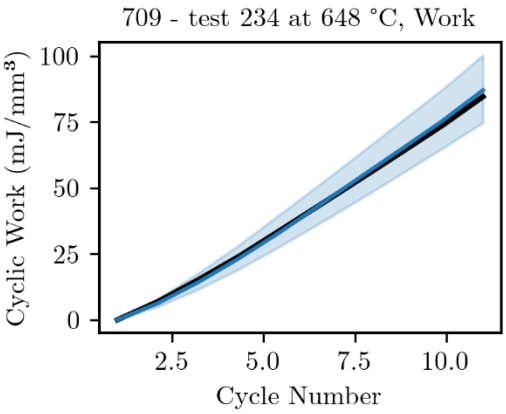
709 - test 234 at 648 °C, Work
Cyclic Work (mJ/mm³)
100
75
50
25
0
2.5
5.0
7.5
10.0
Cycle Number

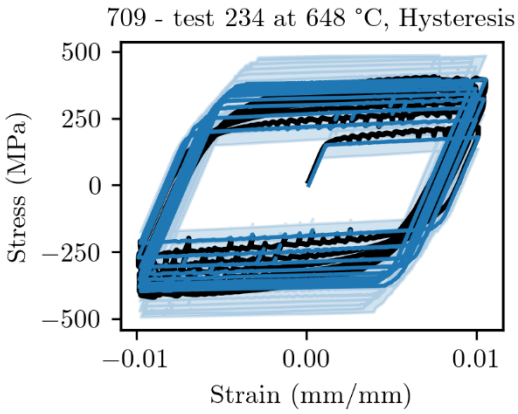
709 - test 234 at 648 °C, Hysteresis
Stress (MPa)
500
250
0
−250
−500
−0.01
0.00
0.01
Strain (mm/mm)

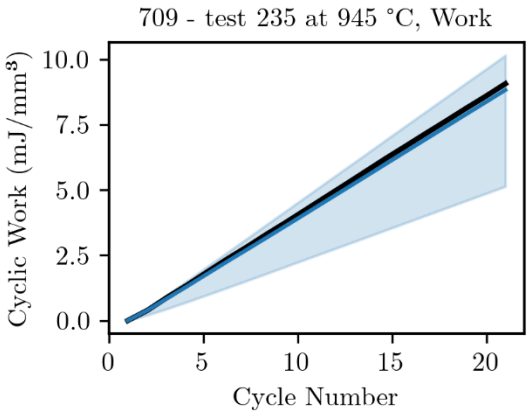
709 - test 235 at 945 °C, Work
Cyclic Work (mJ/mm³)
10.0
7.5
5.0
2.5
0.0
0
5
10
15
20
Cycle Number

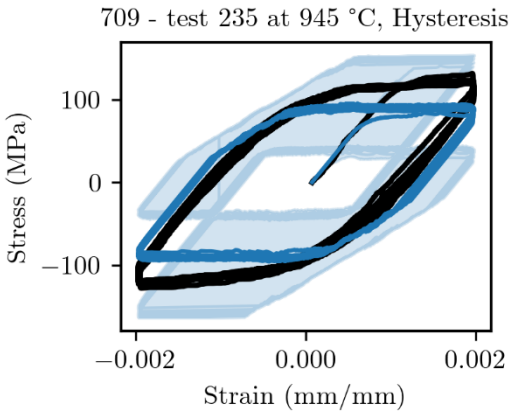
709 - test 235 at 945 °C, Hysteresis
Stress (MPa)
100
0
−100
−0.002
0.000
0.002
Strain (mm/mm)

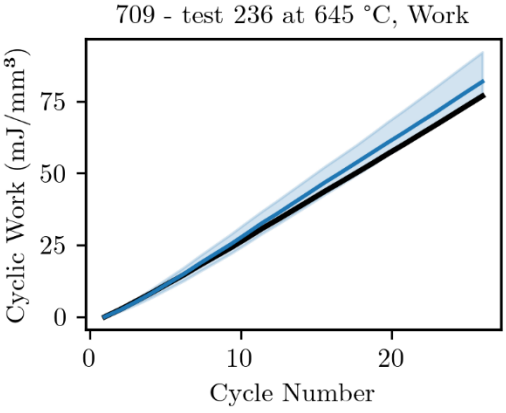
709 - test 236 at 645 °C, Work
Cyclic Work (mJ/mm³)
75
50
25
0
0
10
20
Cycle Number

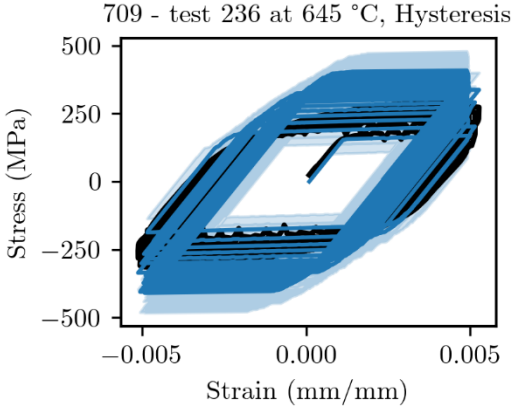
709 - test 236 at 645 °C, Hysteresis
Stress (MPa)
500
250
0
−250
−500
−0.005
0.000
0.005
Strain (mm/mm)

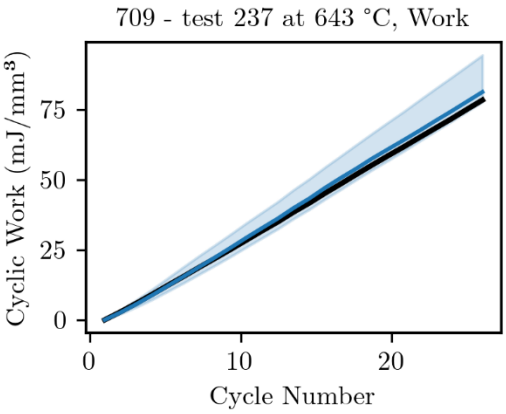
709 - test 237 at 643 °C, Work
Cyclic Work (mJ/mm³)
0
25
50
75
0
10
20
Cycle Number

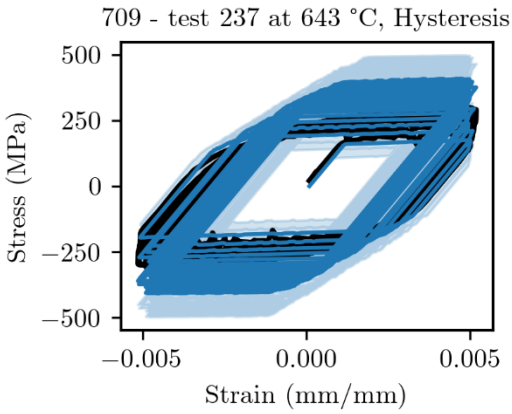
709 - test 237 at 643 °C, Hysteresis
Stress (MPa)
500
250
0
−250
−500
−0.005
0.000
0.005
Strain (mm/mm)

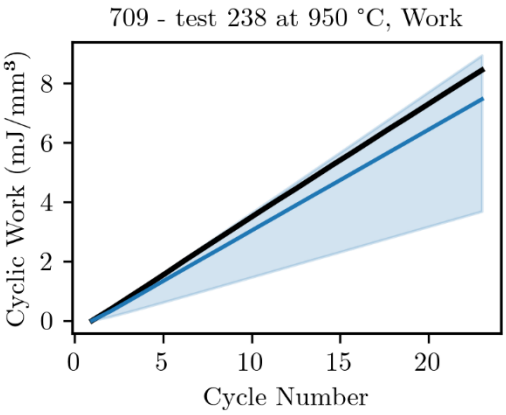
709 - test 238 at 950 °C, Work
Cyclic Work (mJ/mm³)
0
2
4
6
8
0
5
10
15
20
Cycle Number

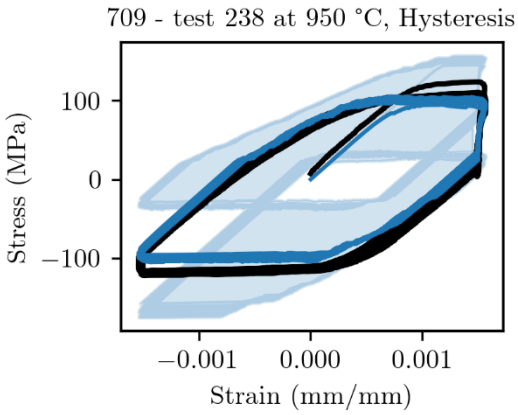
709 - test 238 at 950 °C, Hysteresis
Stress (MPa)
100
0
−100
−0.001
0.000
0.001
Strain (mm/mm)

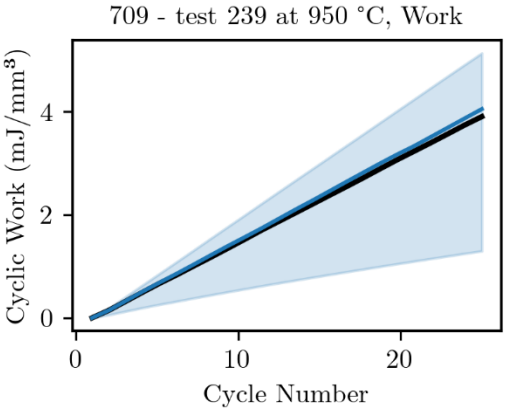
709 - test 239 at 950 °C, Work
Cyclic Work (mJ/mm³)
0
2
4
0
10
20
Cycle Number

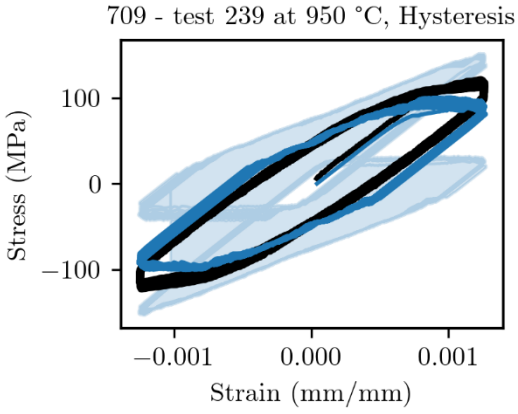
709 - test 239 at 950 °C, Hysteresis
Stress (MPa)
100
0
−100
−0.001
0.000
0.001
Strain (mm/mm)

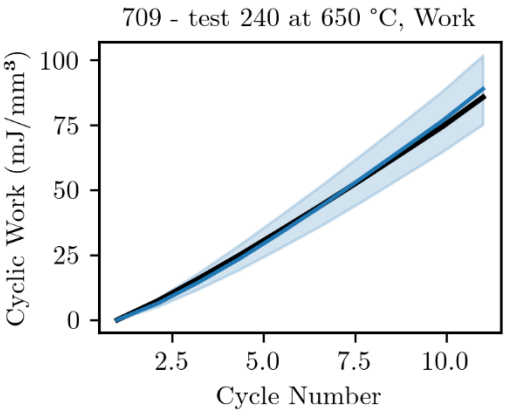
709 - test 240 at 650 °C, Work
Cyclic Work (mJ/mm³)
100
75
50
25
0
2.5
5.0
7.5
10.0
Cycle Number

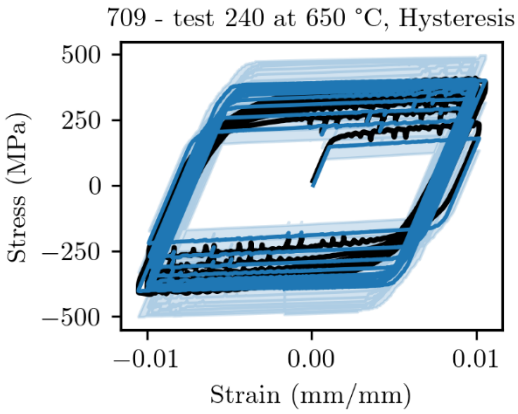
709 - test 240 at 650 °C, Hysteresis
Stress (MPa)
500
250
0
−250
−500
−0.01
0.00
0.01
Strain (mm/mm)

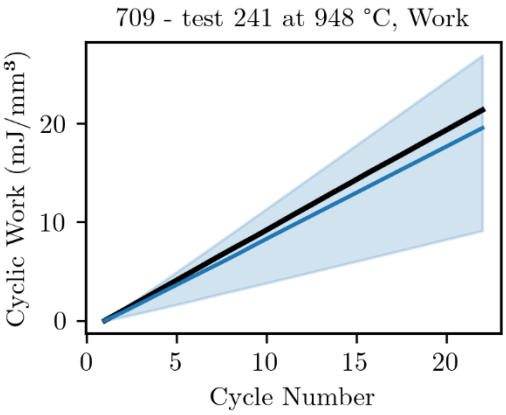
709 - test 241 at 948 °C, Work
Cyclic Work (mJ/mm³)
20
10
0
0
5
10
15
20
Cycle Number

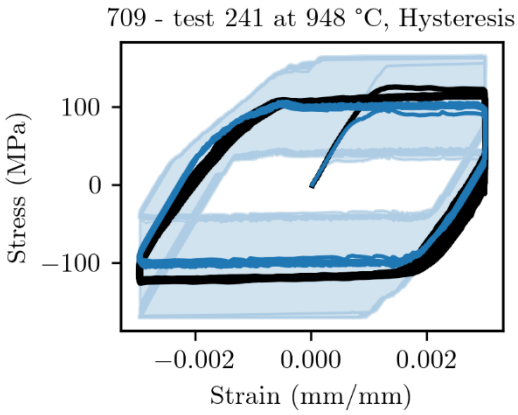
709 - test 241 at 948 °C, Hysteresis
Stress (MPa)
100
0
−100
−0.002
0.000
0.002
Strain (mm/mm)

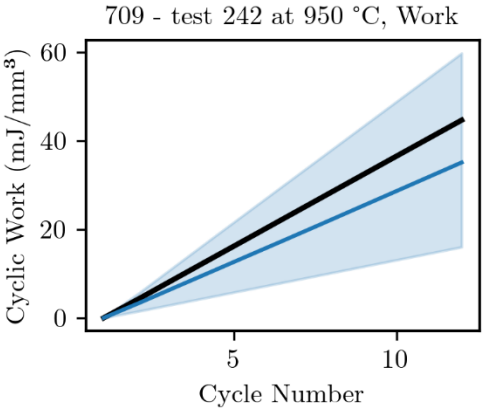
709 - test 242 at 950 °C, Work
Cyclic Work (mJ/mm³)
60
40
20
0
5
10
Cycle Number

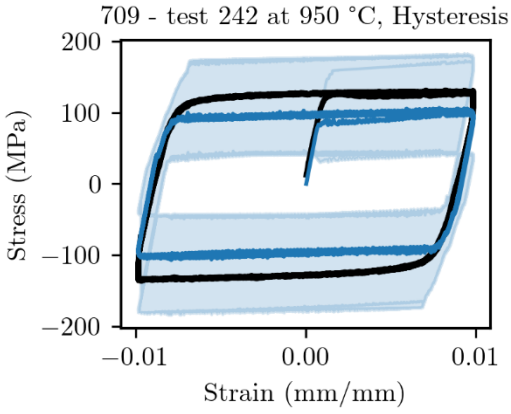
709 - test 242 at 950 °C, Hysteresis
Stress (MPa)
200
100
0
−100
−200
−0.01
0.00
0.01
Strain (mm/mm)

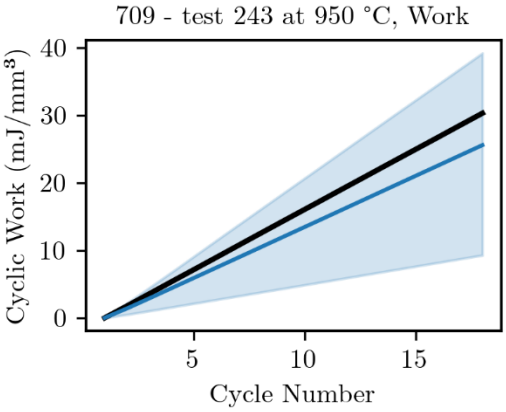
709 - test 243 at 950 °C, Work
Cyclic Work (mJ/mm³)
0
10
20
30
40
5
10
15
Cycle Number

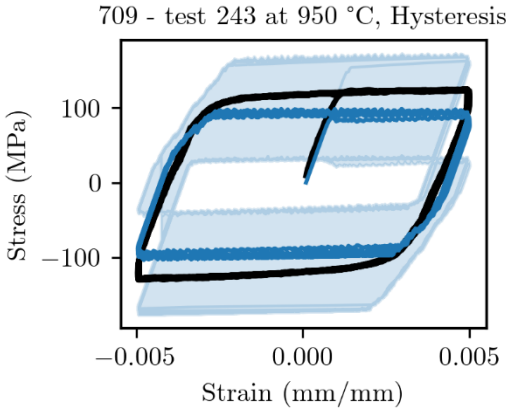
709 - test 243 at 950 °C, Hysteresis
Stress (MPa)
−100
0
100
−0.005
0.000
0.005
Strain (mm/mm)

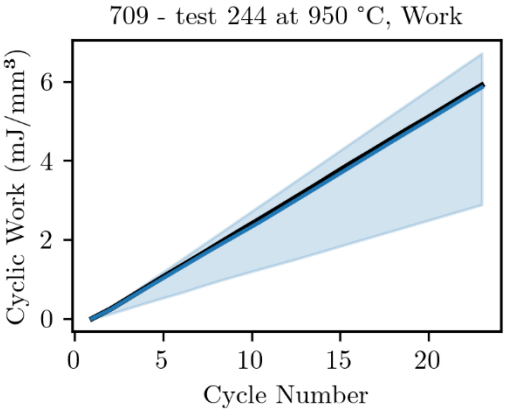
709 - test 244 at 950 °C, Work
Cyclic Work (mJ/mm³)
0
2
4
6
0
5
10
15
20
Cycle Number

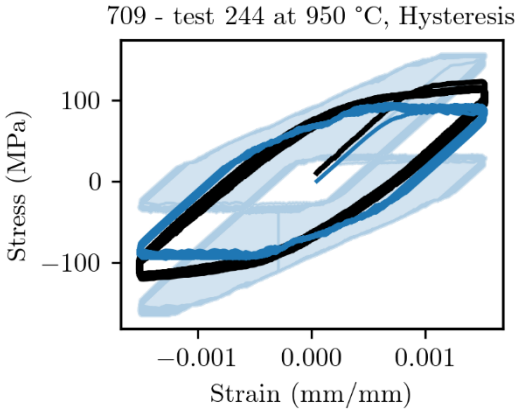
709 - test 244 at 950 °C, Hysteresis
Stress (MPa)
−100
0
100
−0.001
0.000
0.001
Strain (mm/mm)

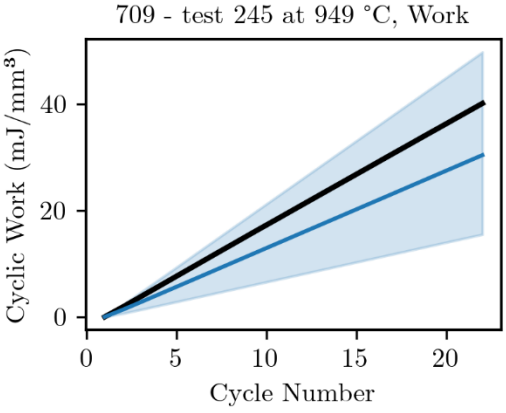
709 - test 245 at 949 °C, Work
Cyclic Work (mJ/mm³)
0
20
40
0
5
10
15
20
Cycle Number

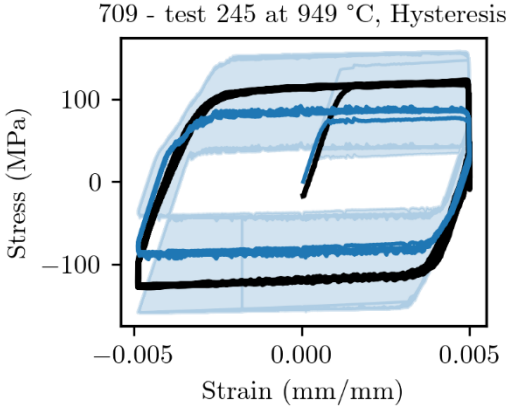
709 - test 245 at 949 °C, Hysteresis
Stress (MPa)
−100
0
100
−0.005
0.000
0.005
Strain (mm/mm)

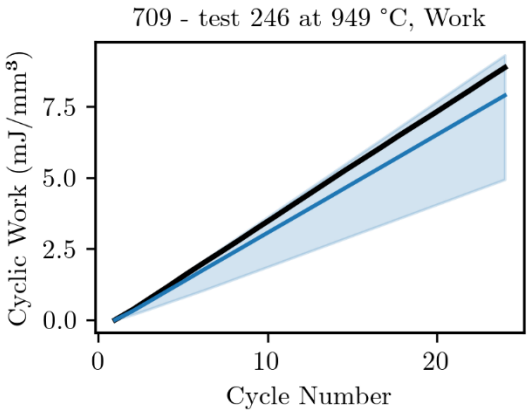
709 - test 246 at 949 °C, Work
Cyclic Work (mJ/mm³)
0.0
2.5
5.0
7.5
0
10
20
Cycle Number

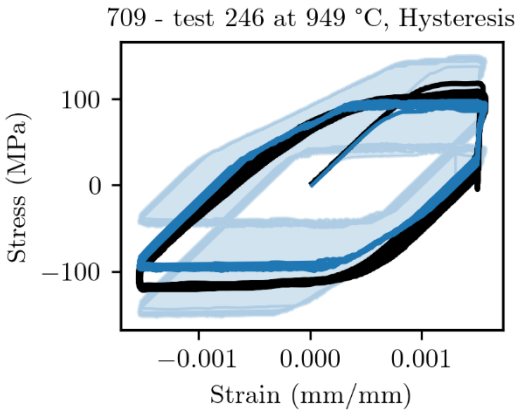
709 - test 246 at 949 °C, Hysteresis
Stress (MPa)
−100
0
100
−0.001
0.000
0.001
Strain (mm/mm)

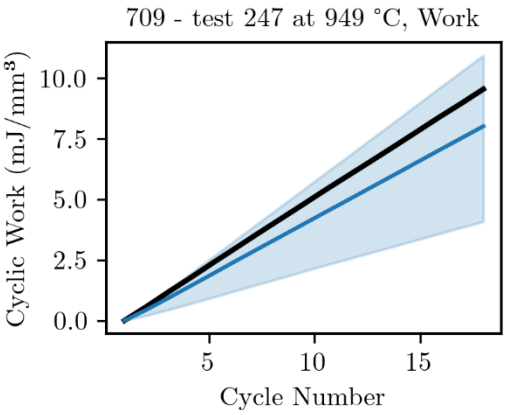
709 - test 247 at 949 °C, Work
Cyclic Work (mJ/mm³)
0.0
2.5
5.0
7.5
10.0
5
10
15
Cycle Number

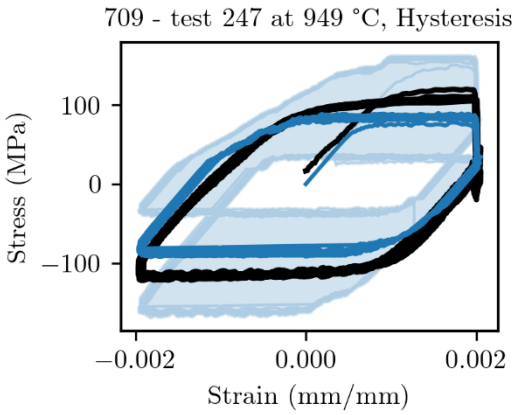
709 - test 247 at 949 °C, Hysteresis
Stress (MPa)
−100
0
100
−0.002
0.000
0.002
Strain (mm/mm)

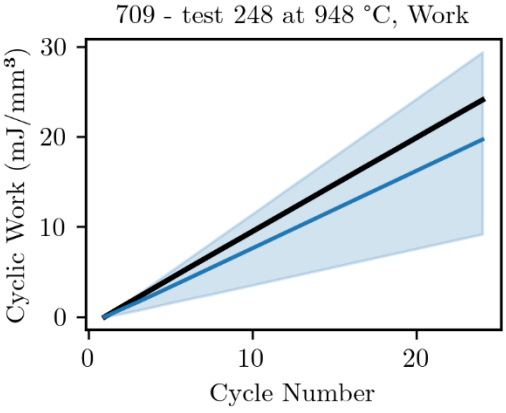
709 - test 248 at 948 °C, Work
Cyclic Work (mJ/mm³)
0
10
20
30
0
10
20
Cycle Number

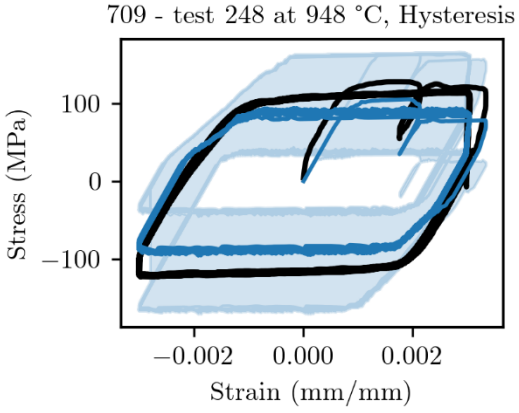
709 - test 248 at 948 °C, Hysteresis
Stress (MPa)
−100
0
100
−0.002
0.000
0.002
Strain (mm/mm)

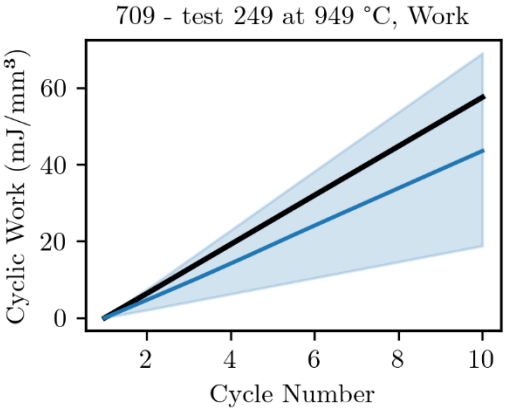
709 - test 249 at 949 °C, Work
Cyclic Work (mJ/mm³)
0
20
40
60
2
4
6
8
10
Cycle Number

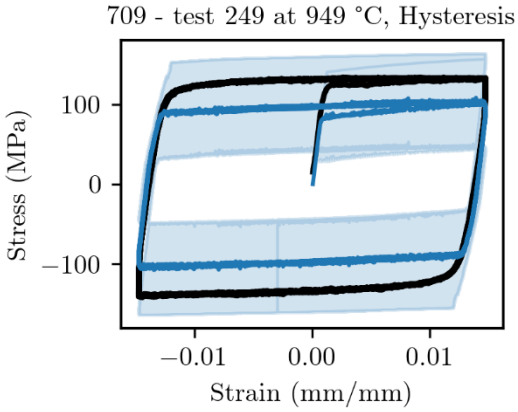
709 - test 249 at 949 °C, Hysteresis
Stress (MPa)
−100
0
100
−0.01
0.00
0.01
Strain (mm/mm)

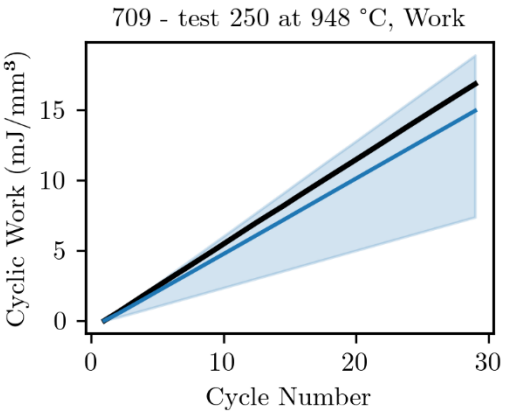
709 - test 250 at 948 °C, Work
Cyclic Work (mJ/mm³)
0
5
10
15
0
10
20
30
Cycle Number

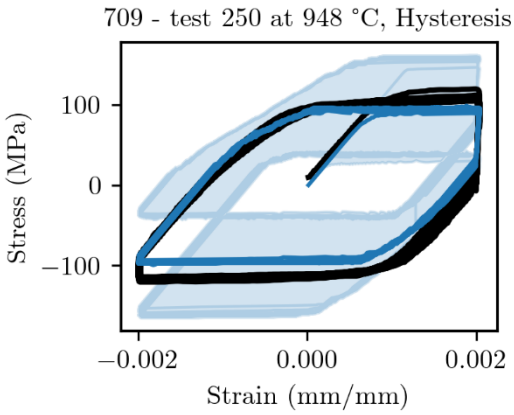
709 - test 250 at 948 °C, Hysteresis
Stress (MPa)
−100
0
100
−0.002
0.000
0.002
Strain (mm/mm)

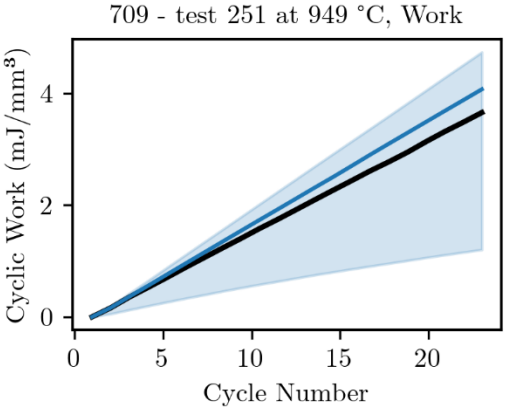
709 - test 251 at 949 °C, Work
Cyclic Work (mJ/mm³)
0
2
4
0
5
10
15
20
Cycle Number

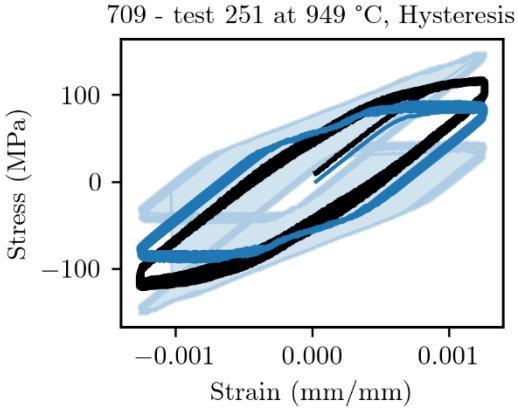
709 - test 251 at 949 °C, Hysteresis
Stress (MPa)
−100
0
100
−0.001
0.000
0.001
Strain (mm/mm)

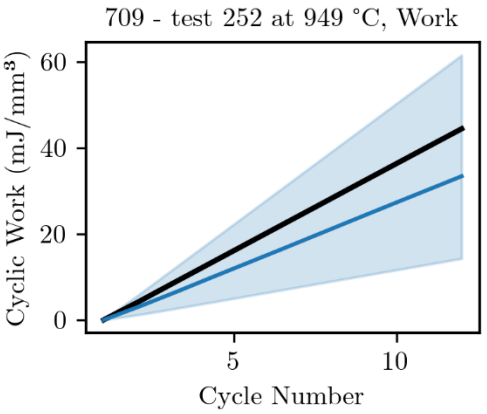
709 - test 252 at 949 °C, Work
Cyclic Work (mJ/mm³)
0
20
40
60
5
10
Cycle Number

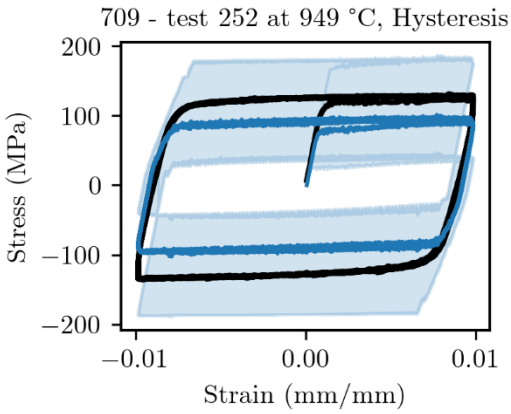
709 - test 252 at 949 °C, Hysteresis
Stress (MPa)
200
100
0
−100
−200
−0.01
0.00
0.01
Strain (mm/mm)

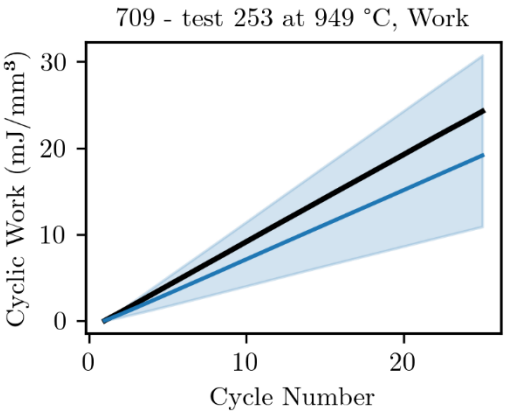
709 - test 253 at 949 °C, Work
Cyclic Work (mJ/mm³)
0
10
20
30
0
10
20
Cycle Number

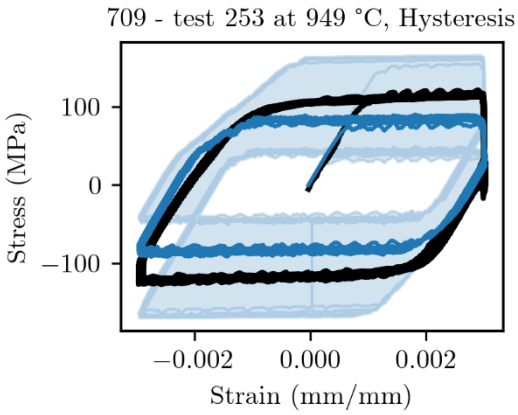
709 - test 253 at 949 °C, Hysteresis
Stress (MPa)
100
0
−100
−0.002
0.000
0.002
Strain (mm/mm)

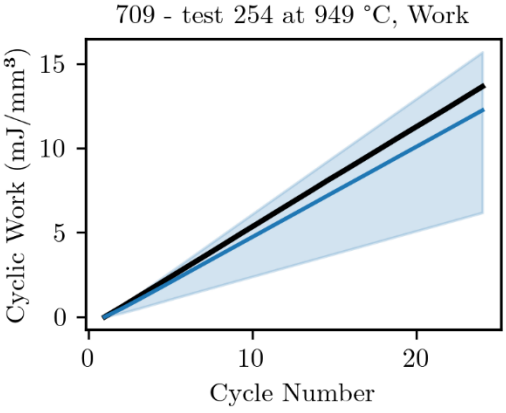
709 - test 254 at 949 °C, Work
Cyclic Work (mJ/mm³)
0
5
10
15
0
10
20
Cycle Number

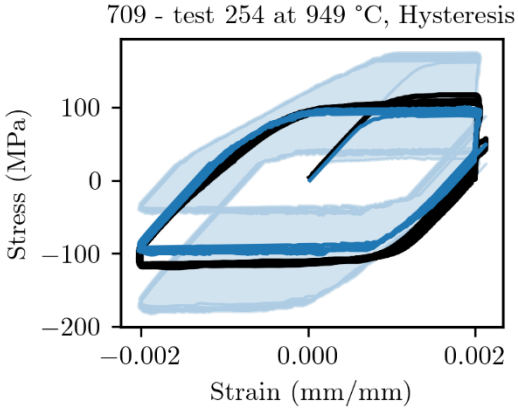
709 - test 254 at 949 °C, Hysteresis
Stress (MPa)
100
0
−100
−200
−0.002
0.000
0.002
Strain (mm/mm)

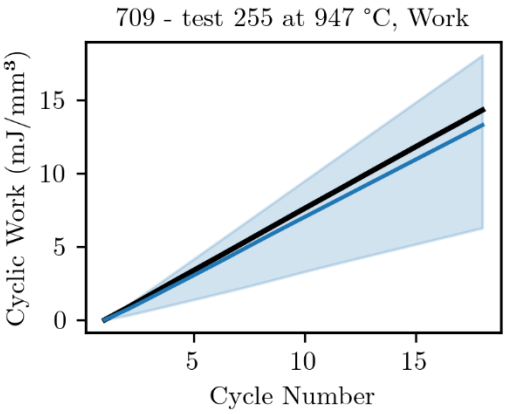
709 - test 255 at 947 °C, Work
Cyclic Work (mJ/mm³)
0
5
10
15
5
10
15
Cycle Number

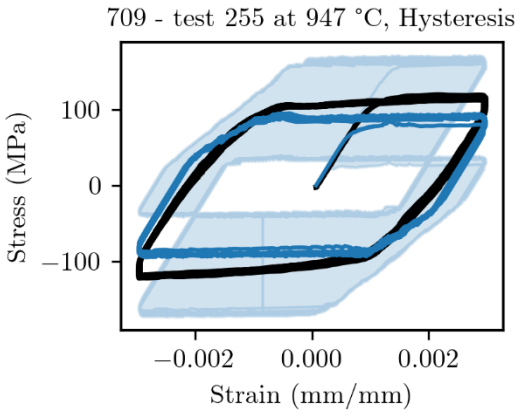
709 - test 255 at 947 °C, Hysteresis
Stress (MPa)
100
0
−100
−0.002
0.000
0.002
Strain (mm/mm)

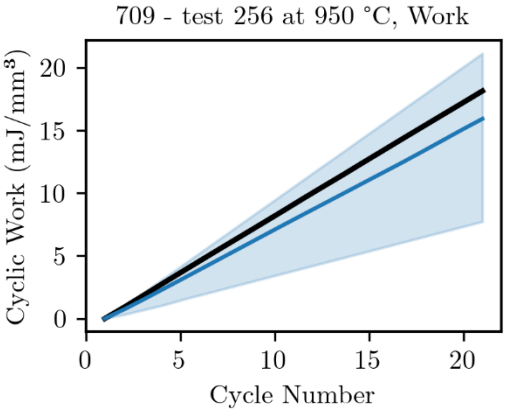
709 - test 256 at 950 °C, Work
Cyclic Work (mJ/mm³)
0
5
10
15
20
0
5
10
15
20
Cycle Number

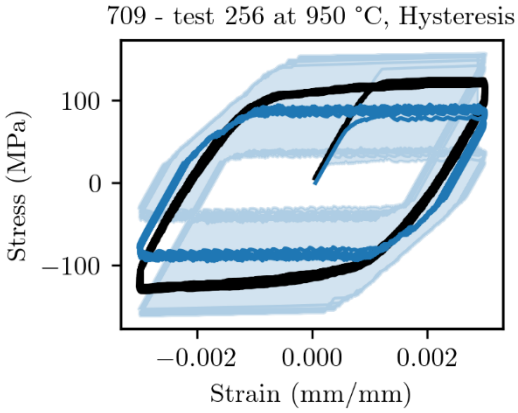
709 - test 256 at 950 °C, Hysteresis
Stress (MPa)
100
0
−100
−0.002
0.000
0.002
Strain (mm/mm)

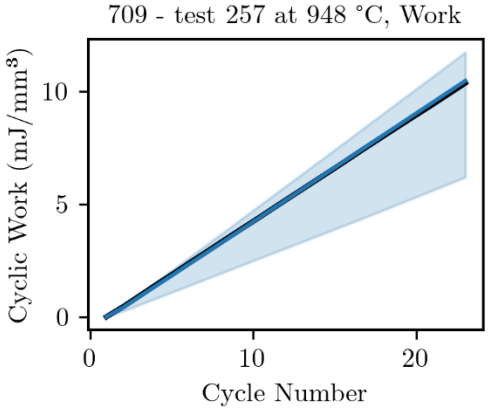
709 - test 257 at 948 °C, Work
Cyclic Work (mJ/mm³)
0
5
10
0
10
20
Cycle Number

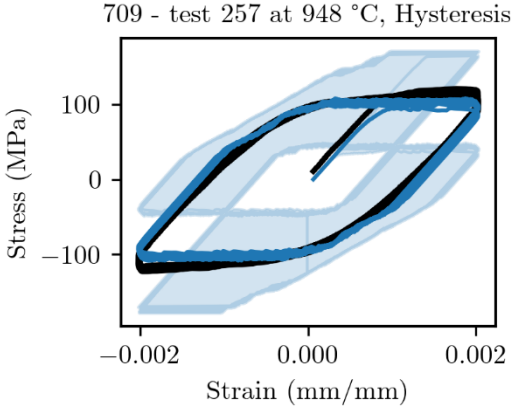
709 - test 257 at 948 °C, Hysteresis
Stress (MPa)
100
0
−100
−0.002
0.000
0.002
Strain (mm/mm)

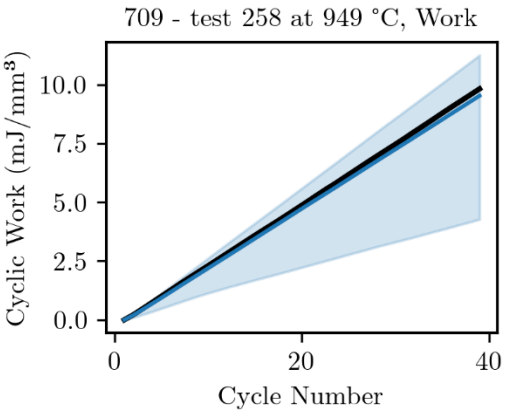
709 - test 258 at 949 °C, Work
Cyclic Work (mJ/mm³)
10.0
7.5
5.0
2.5
0.0
0
20
40
Cycle Number

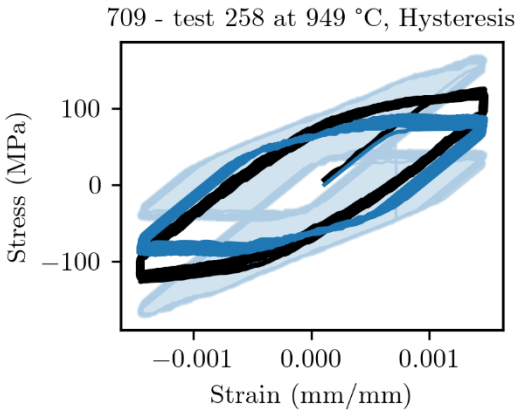
709 - test 258 at 949 °C, Hysteresis
Stress (MPa)
100
0
−100
−0.001
0.000
0.001
Strain (mm/mm)

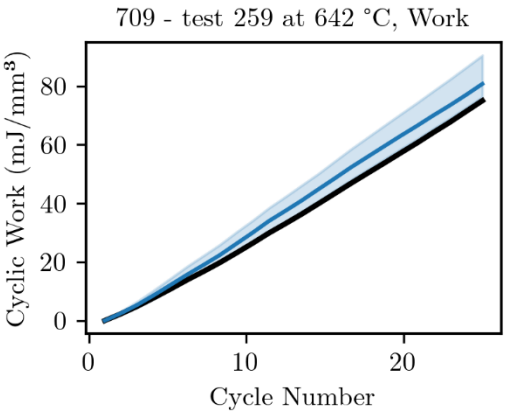
709 - test 259 at 642 °C, Work
Cyclic Work (mJ/mm³)
80
60
40
20
0
0
10
20
Cycle Number

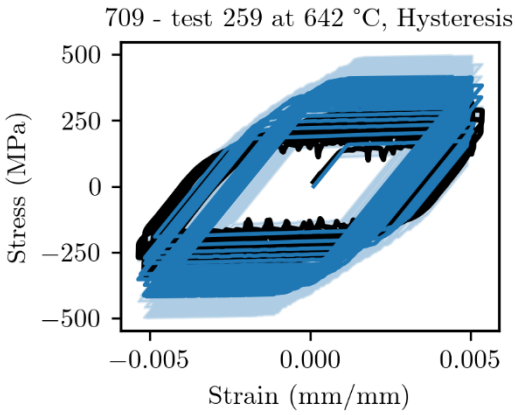
709 - test 259 at 642 °C, Hysteresis
Stress (MPa)
500
250
0
−250
−500
−0.005
0.000
0.005
Strain (mm/mm)